Epileptic responses in marmosets induced by knockdown of CREB Regulated Transcription Coactivator 1 (CRTC1)

Yuki Nakagami*[1], Misako Komatsu*[1,2], Ken Nakae*[3], Masanari Otsuka[1,2], Junichi Hata[4], Hiroaki Mizukami[5], Hiroshi Takemori[6], Shin Ishii[3], Hideyuki Okano[4], Akiya Watakabe[1,2], Tetsuo Yamamori[1,2**]

[1]Laboratory of Molecular Analysis for Higher Brain Function, Center for Brain Science, RIKEN, Japan

[2]Laboratory of Haptic Perception and Cognitive Physiology, Center for Brain Science, RIKEN, Japan

[3]Integrated Systems Biology Laboratory Department of Systems Science, Graduate School of Informatics, Kyoto University; Kyoto, Japan

[4]Brain Image Analysis Unit, RIKEN Center for Brain Science, Wako, Japan

[5]Division of Genetic Therapeutics, Center for Molecular Medicine, Jichi Medical University, Shimotsuke, Japan

[6]Department of Chemistry and Biomolecular Science, Gifu University, Gifu, Japan

*These authors contributed equally.

** Corresponding author

Laboratory of Haptic Perception and Cognitive Physiology, Center for Brain Science, RIKEN,

2-1 Hirosawa, Wako, Saitama, 351-0198, Japan

E-mail: tetsuo.yamamori@a.riken.jp

PHONE: 81-5035026248

FAX: 81-484672539

Abstract

Epilepsy is a major neurological disorder. Despite the major contribution of animal models to the development of anticonvulsant drugs, 20-30% of epilepsy patients still fail to achieve adequate seizure control. Novel animal models are needed for the development of new drugs. Here we report *CRTC1* KD-induced epileptic response by short hairpin (shRNA) RNA injection into marmoset V1. Three local injections of *shCRTC1* induced *cFOS* expression beyond the injection sites. Real-time analysis of cortical electrocorticography revealed transient changes in high frequency oscillations throughout the cortex, and a second lesion was observed in the temporal lobe by MRI and post-mortem histology. *shCRTC1* knockdown marmosets showed severe lesions surrounding the injection site several months after the injection, while glial cell activations appeared even before IEG induction could be detected one month after the *shCRTC1* injection. These features suggest the utility of the *shCRTC1* KD marmoset in the study of focal and structural epilepsy.

Main

Epilepsy is a major neurological disorder, affecting approximately 0.4-1% of the global population[1, 2]. Despite the invaluable contributions made by animal models combined

with advances in drug discovery[3-9], there is a subgroup of epilepsy patients, 20% to 30%, who do not achieve seizure control or experience intolerable adverse effects[3, 4, 9]. As most current epilepsy models are based on abnormal electrical potential changes, there is a growing demand to cultivate a diverse range of animal models, accurately representative of the 15 distinct epilepsy subtypes[10] in order to facilitate the adoption of updated[11] approaches in both research and drug development.

We previously found immediate early gene (IEG) expression in the primary visual cortex (V1) of the marmoset[12] and simultaneous CRTC1 transient nuclear translocation and dephosphorylation of cAMP response element-binding protein (CREB) in V1 neurons following light stimulation (LS) in marmosets (unpublished data). Here, we report unexpected widespread *cFOS* expression in the injected hemisphere *CRTC1* KD caused by short hairpin RNA (shRNA) injections. A series of experiments ranging from histological analysis to cortical electrocorticography (ECoG) and magnetic resonance imaging (MRI) were performed.

The marmoset ECoG is advantageous for cortical-wide monitoring with high spatiotemporal resolution[15-17] and long recording times. It allowed us to uncover sequential real time events after *shCRTC1* injection, revealing that the cellular spread of neurodegeneration was localized to the injected area by activation of surrounding glial

cells, while epileptic neuronal activity spread from the injection site throughout the cortex and abnormal functional connectivity was observed. Epileptic foci migrated to the temporal cortex, and functional connectivity eventually reached a steady state several months after injection. These features make this a strong candidate for a useful animal model of focal and structural epilepsy to study epileptogenesis in real time from onset.

Results

This study was prompted by our unexpected finding that *shCRTC1* KD induced unusual *cFOS* expression beyond the injection site. We made five shRNA sequences for KD of marmoset *CRTC1* (see Method), with *shCRTC1*#1 and #2 generated against the coding sequences and from #3 to #5 against the 3'-UTR sequences. *shCRTC1*#1 and #2 showed the strongest and second strongest *CRTC1* KD effects, respectively (Extended Data Fig. 1a). We used 10 marmosets in this study. The rearing conditions of these marmosets are described in the respective experiments and figures (see Supplementary Table 1).

shCRTC1 injection at three local sites in V1 provides broad IEG expression

shCRTC1#1 was injected at three sites in the left V1. A control scrambled sequence

(*shscr)* was also injected at one site and two sites in the right and left V1, respectively. As in the previous experiments that we first followed, four weeks after shRNA injection, one eye was injected with tetrodotoxin (TTX) and subjected to dark rearing (DR) for 41hr followed by LS for 24 min (Figs. 1a and b). In contrast to *shscr*, *shCRTC1*#1 injection abolished CRTC1 protein expression (Fig. 1c upper panel). In the control hemisphere with a single *shscr* injection, *cFOS* expression showed an ocular dominance column (ODC)-like pattern (Figs. 1c and d, bottom right and right, respectively). In contrast, aberrant *cFOS* expression was observed throughout V1 and V2 in the *shCRTC1*-injected hemisphere (Figs. 1c bottom left and 1d left). *cFOS* mRNA expression in left V1 was strongest in layer 2, with the ODC pattern obscured by the abnormal cFOS expression and very different from the right hemisphere that showed the typical *cFOS* induction pattern observed under TTX and LS conditions[12]. These results demonstrated the widespread abnormal expression of *cFOS* in the *shCRTC1#1* injected visual cortex independent of visual input.

We examined the expression of several other IEGs at a site distant from the injection site within V1 (Fig. 1e). The changes in the expression patterns of *ARC*, *ZIF268* (*EGR1* or *NGFIA*), and *NUR77 (NR4A1)* showed almost the same characteristics as those seen in the *cFOS* expression pattern. The strong expression in layer 2 and the distribution

with little ODC borders were different from those seen in the right V1. *NURR1* (*NR4A2*), a subtype of layer 6 neurons[18] and the CREB downstream gene, showed activity-dependent gene expression in layers besides layer 6 at approximately 2hr after LS (data not shown). In the left V1 of Monkey 1, *NURR1* was aberrantly expressed only in the upper layer 2, with no abnormal expression pattern in other layers. In addition, the expression patterns of other retinal activity-dependent genes, *HTR1B* and *HTR2A*[12], showed ODC-like patterns independent of *shCRTC1* injection (data not shown). This suggests that shCRTC1 injection induced aberrant IEG expression in V1 independent of retinal activity.

A similar IEG expression pattern in the right V1 to those expressed in *shCRTC1#1* noninjected marmosets was observed under the same DR and LS conditions. LS-induced cFOS protein in the right V1 was undetectable at 24 min after LS, but significant cFOS protein expression was observed in layer 2 in the left V1 (Fig. 1e, right), being consistent with the abnormal IEG expression in the left hemisphere independent of LS.

In the region surrounding the *shCRTC1*#1 injection site, *ARC* and *ZIF268* (data not shown) were widely and uniformly expressed in addition to *cFOS* (Fig. 1c, bottom left). *NUR77* expression was markedly reduced except in layer 2 at the *shCRTC1*#1 injection

sites (Extended Data Fig. 1c), and the *NURR1* expression was slightly reduced in layer 6a and strongly reduced in layer 6b (Extended Data Fig. 1d). These results suggest that local reduction of CRTC1 altered local IEG expressions, which further affected much wider areas of the same hemisphere by the three-site injection of *shCRTC1*#1 in Monkey 1.

CRTC1 KD at one or two sites in one hemisphere induces only limited local IEG expression

AAV injection sites occupy a fraction of V1: Each site is approximately 1 mm in diameter in the marmoset brain, which measures approximately 3 cm x 2 cm (M-L)[19] (Fig. 1a). We examined how a reduced number of injection sites affected IEG induction in monkeys 2 and 3 (Figs. 2a and 2b). In Monkey 2, intense *cFOS* expression occurred at both injection sites and nearby Sirius-negative cells (especially in layers 2/3) but not beyond (Fig. 2a and Extended Data Fig. 2). We assessed other IEGs (*ARC*, *ZIF268*, *NURR1*). Similar to *cFOS*, *ARC* and *ZIF268* were uniformly strongly expressed in both Sirius-positive and -negative cells around the injection site. No genes showed a strong signal in upper layer 2 as seen in Monkey 1. *NURR1* was attenuated only in layer 6 of the injection site and there was no *shCRTC1*-induced expression (Extended Data Fig. 2).

Monkey 3 underwent normal rearing for 4 weeks after AAV injection, followed by DR and LS before sacrifice (Fig. 2b).

LS induced broad *cFOS* mRNA expression, with stronger intensity around the right V1 shCRTC1 injection site (Fig. 2c, middle). In contrast, more limited *cFOS* and *ARC* induction and *NUR77* reduction were observed at the left induction site (Fig 2d middle panels). Note that in Monkey 1 *NUR77* was strongly reduced at the injection site, but the induction outside of the injection site was observed as described above (Fig. 1e and Extended DATA Fig. 1c). Aberrant cFOS protein expression was observed at the left injection sites (Fig. 2c, middle and right panel panels). Taken together, these results suggest that when *shCRTC1*#1 injected into more clustered cells, the excitatory activity spreads more to surrounding cells.

Expression of cell lesion and apoptosis related markers 24 days after injection in Monkeys 1, 2 and 3

In the process of histological analysis, we noticed neuronal loss conspicuous only at the *shCRTC1* injection sites in Monkey 1. We examined the extent of neuronal lesions induced by *shCRTC1* injection, together with other cell injury or death markers. Nissl staining revealed microglial accumulation and tissue damage and NeuN signals were

reduced at the *shCRTC1*-injected site (Extended Data Fig. 3b), little or no signal reduction by *shscr* injections was seen (data not shown). The NeuN signal was attenuated in *shCRTC1*#1-infected cells and was markedly reduced in areas of severe tissue damage. Consistent with Nissl staining, IBA1 signal, indicating microglial activation, was observed at the center of the injection site. In contrast, the GFAP signal indicated astrocyte activation around and near the edge of the injection site (Extended Data Fig. 3a, middle). Cell death signals detected by TUNEL staining, were in the central region of the *shCRTC1*#1 injection site (Extended Data Fig. 3c). No TUNEL signal was observed at the *shscr* injection site (data not shown). Because CRTC1 activation and CREB phosphorylation are associated but independent processes with synaptic activity[20], we examined the phosphorylation status of CREB at SER133 by IHC. Significant phosphorylated CREB signals were observed in neurons injected with *shCRTC1* (Extended Data Fig. 3d). We also performed a series of analyses on neurodegeneration in Monkeys 2 and 3. Nissl staining showed less neuronal loss and tissue damage in the two Monkeys than Monkey 1. Correspondingly, the immunostaining signals for IBA1 and GFAP were weaker (Extended Data Figs. 3a and 4a). NeuN signals were also reduced at *shCRTC1* injection sites, but only a few TUNEL signals were observed. (Extended Data Figs. 4b and 4c). pCREB signals were also

observed at the s*hCRTC1* injection sites in both monkeys (data not shown). These expressions of cell death related markers raised the question of how they relate to the IEG inductions. Therefore, we performed the experiments shown in the following sections.

Expression of cell death related markers and IEG induction

To evaluate the effect of *shCRTC1*s besides *shCRTC1*#1, we injected different *shCRTC1*s (See Method) into V1 of Monkey 4. *shCRTC1*s and *shscr* injections, 2 days after TTX injection with DR, LS for 24 min followed by sacrifice (Fig. 3a) in Monkey 4, similar to Monkey 1. All *shCRTC1*s, but not *shscr*, reduced CRTC1 signals (Fig. 3b). Cell death related and IEG expression markers were examined as follows. Variable NeuN reduction occurred among *shCRTC1*s on injection sites. *shCRTC1*#1, #2, and #4 caused greater NeuN reduction than #3 and #5 (Fig. 3c). Histological damage was prominent with *shCRTC1*#1 and #2 compared to #5 (Fig. 3d). Strong IBA1 signals were present at sites #1, #4, and #2, with complementary GFAP signals (Fig. 3e). *ShCRTC1*#1 and #2 which caused more neuronal damage, also showed phosphorylated CREB signals (Fig. 3f). Decreased *cFOS* mRNA expression was observed at all *shCRTC1*s injection sites (e.g., see *shCRTC*1#1 and #5; Fig. 3g), with no abnormal

IEG expressions.

After 41hr of monocular TTX injection, LS induced *cFOS* expression as an ODC-like pattern in V1, indicating that only half of the V1 areas were activated compared to normal marmosets under NR and LS. The reduction in *cFOS* at the *shCRTCs*' injected sites may be due to the reduced activated area of half of the *shCRTC1* injected region in V1 because of monocularly injected TTX in Monkey 4. This may be consistent with the finding that less *shCRTC1*#1 injection resulted in less *cFOS* induction (Figs. 2c, 2d).

Monkey 8, normal rearing, received *shCRTC1*#2 and #3 injections at one site each, and *shCRTC1*#5 at two (Fig. 3h). IEG expression was reduced at *shCRTC1* but not *shscr* injected sites (*ZIF268*, Fig. 3h) without abnormal IEG expression. Monkey 9 confirmed this with *shCRTC1*#2 and #5 injections (Supplementary Table 1).

Severe neuronal loss occurred by *shCRTC1*#1 and #2. IBA1 signals were central, GFAP signals peripheral at #2 site. TUNEL signals were present at other *shCRTC1* sites, highest at #2 (Fig. 3i). Widespread *shCRTC1*-induced IEG expression was also seen in monkey 7 with *shCRTC1*#1 injection, along with *shCRTC1*#2 and #3 at one or two sites that cannot cause such IEG inductions alone (Supplementary Table 1). To characterize shCRTC1#1 and #2, *shCRTC1*#1 influenced more IEG induction, while *shCRTC1*#2 may have influenced more tissue damage.

shCRTC1#2 induced _cFOS_ expression beyond the injection site when injected at 2 or 3 sites

Even if the excitatory activity evoked is weak in individual cells, it becomes stronger as the infected region becomes larger (Figs. 2 and 2d). We further tested this possibility by using *shCRTC1*#2. Indeed, when *shCRTC1*#2 was injected at two sites in one V1 hemisphere, *cFOS* expression was observed beyond the injection site (Extended Fig. 5), with increased IBA1 and decreased NeuN signals at the injection sites (Extended Fig. 6). Injection of *shCRTC1*#2 at three sites caused further decreased NeuN expression and increased IBA1 and TUNEL signals; however, the *cFOS* expression was rather restricted to the periphery of the injection site (Extended Data Figs. 5b).

Monkey 7, injected with one site of *shCRTC1*#1, two sites of *shscr,* and one and two sites of s*hCRTC1*#2 and #3, respectively, in one hemisphere (see Supplementary Table 1), showed widespread IEG expression beyond the *shCRTC1*#1 injected sites as seen in Monkey 1, despite one site injection of *shCRTC1*#1 on each hemisphere. As described above, the activity induced by injection of *shCRTC1*#1 was not strong when the size of the infected cells was limited but was increased to unusually strong levels with multiple injection sites. Due to the lower KD efficiency of other *shCRTC1*s than *shCRTC1*#1,

they would be unable to induce abnormal IEG expression by single injection alone. However, a wider IEG expression was observed by injecting *shCRTC*#1 at one site and other *shCRTC1*s at multiple nearby sites in Monkey 7. This suggests that *shCRTC1*s other than *shCRTC1*#1 can also contribute to aberrant expression of IEGs when the infected cells and sites are clustered.

Occurrence of abnormal High-frequency activity in *shCRTC1* KD marmosets

Through the histological analysis that showed wider expression of IEG, we consider that these may cause abnormal cortical activation. The abnormal IEG expression in layer 2 of Monkey 1 was similar to the IEG pattern reported in human tissue from epilepsy patients[21]. In addition, the histological observations described above, such as the decrease in NeuN-positive cells, strong positive GFAP signals, and neuronal loss one month after three *shCRTC1*#1 injections, were also consistent with those seen in human epilepsy. We hypothesized that local injection of *shCRTC1*#1 into V1 induces abnormal excitatory activity in a cluster of infected neurons, which in turn causes epileptic activity that spreads throughout the cortex. To test this hypothesis, long-term recordings of cortical neuronal activity were performed in two *shCRTC1* KD marmosets (Monkeys 5 and 6). After injection of *shCRTC1*#1 at three adjacent sites in V1, ECoG

electrodes[22] were placed over the lateral hemisphere on the dura mater of Monkeys 5 and 6 on the same day and 1 week after injection, respectively (Fig. 4a). After recovery, Monkeys 5 and 6 underwent ECoG recordings for 1-2hr per day and behavioral observations for 2 and 5 months, respectively. During the recordings, the monkeys sat in a primate chair without performing any task and were exposed to a variety of pure tones used in the previous study[23] for the first 20 min. In addition to electrophysiological monitoring, preoperative *in vivo* MRI (T2-weighted imaging) and postmortem *ex vivo* MRI (T2-weighted imaging and diffusion MRI (dMRI)) were performed to examine structural changes (Fig. 4a). Cortical activity was observed for 2 months in Monkey 5 and up to 5 months after the start of observation in Monkey 6 (Fig. 4b). For quantitative analysis of the ECoG signal, we focused on the High-frequency (80-200 Hz) range obtained during the first 15 minutes of each day's recording, because High-frequency oscillations (HFOs) are considered a biomarker for epileptic foci[21, 24, 25]. Examination of the High-frequency activity (HFA) (80-200 Hz, >3 SD) from all electrodes revealed that it occurred in multiple locations in V1, at the injection site, and even in regions of uninfected sites, and decreased 5 weeks after injection in both *shCRTC1* KD marmosets (Fig. 4c-e). We then defined HFA spreading over more than 50% of the electrodes as cortical-wide HFO (cwHFO) (Figs. 4c, 4d and Extended Data Figs. 7 and 8). To identify

the cwHFO onset site, we calculated the average value of the HFA 250ms immediately preceding the cwHFO. Early after *shCRTC1*#1 injection, HFA was observed in V1 preceding cwHFO, but by 4 weeks after the injection, these HFAs had decreased, and the HFA in the temporal cortex tended to precede the cwHFO (Figs. 4c, d and f, Extended Data Fig. 9 and Supplementary Videos 1 and 2). In addition, behavioral monitoring suggests that these HFAs are associated with behavioral outcomes. Both marmosets tended to look around and vocalize during periods of strong occipital HFA occurred but were stationary during periods of strong temporal lobe HFA occurred (visual observations). In addition, buccal hair ruffling was observed approximately two months after injection (Supplementary Video 3).

Reorganization of functional networks in epilepsy

To understand the significance of the changes in HFA patterns, we examined the daily functional network by calculating the correlations between each electrode on each recording day and averaging the correlations over all days (Fig. 5a). The early recordings tended to show dissociations of the functional connectivity, or correlations, from the averaged functional connectivity after injection. In contrast, later recordings showed that the functional connectivity was close to the average (Fig. 5b). To further

investigate this variability, we compared the daily values of the average functional connection between presumptively defined cortical regions (see Methods). We found that the functional connectivity within 5 weeks after injection tended to differ from the average (Fig. 5d). Among the connections, the value of the V1-V1 (other regions within V1) connection was significantly reduced in both monkeys (Fig. 5e). This suggests that the local functional connectivity in the visual cortex decreased immediately after *shCRTC1*#1 injection and reorganized to a stable level 5 weeks after injection.

Progressive cell death at *shCRTC1*#1 injection sites associated with epileptogenesis

We performed postmortem histological analysis of Monkeys 5 and 6, two and five months after *shCRTC1*#1 injections, respectively, to examine histological changes occurred after long-term abnormal cortical activity. In both Monkeys 5 and 6, the expression pattern of *cFOS* mRNA showed almost the same distribution as in the NR condition, except that cells expressing relatively strong *cFOS* were sparsely observed in the upper layer 2 throughout the hemisphere (Fig. 6a). Other IEGs examined (e.g., *ARC* and *BDNF*) were also similar (Fig. 6b). At the injection sites, sparse but relatively strong *cFOS* expression was observed around the *shCRTC1#1* but not *shCRTC1*#2 injection site in Monkey 5 (Figs. 6a, 6c and 6f). No significant *cFOS* signal was

observed at the *shCRTC1*#1 injection site in Monkey 6 (data not shown).

In Monkey 5, many TUNEL signals were observed at the center of *shCRTC1*#1 injection sites where many Sirius-positive neurons were observed. On the other hand, strong IBA1 signals and a mesh-like structure with GFAP signals were observed only at the edge of the injection site where Sirius-positive neurons were observed (Fig. 6d). The strong IBA1 signal suggested undergoing phagocytosis of dying neurons (Fig. 6d). GFAP signals forming reticular structures indicate activated astrocytes undergoing gliosis (Fig. 6d). This suggests that cell death was well advanced before two months after injection, beyond the time point at which we examined histology. Monkey 6 was sacrificed five months after injection. Most of the neuronal loss was within the surrounding wall. GFAP signals also disappeared in the center of the injection, forming a glial scar[23] (Fig. 6e). As shown by Nissl staining, neurons in most injection sites were completely lost, and TUNEL signals were not observed at the injection site or its periphery (Fig. 6e).

Postmortem MRI T2 images of Monkey 5 showed signal loss in part of the right temporal lobe (Fig. 6h), but no such signal loss in *in vivo* MRI T2 images taken before *shCRTC1*#1 injection; Nissl staining also revealed columnar-like cell death in the right temporal lobe of Monkey 5 (Fig. 6i). We detected signals for GFAP and IBA1 (Fig. 6j

and 6k, respectively), but no TUNEL-positive neurons (data not shown). These results suggest that the cell death events may peak about two months after the *shCRTC1*#1 injection and most cells die out in the injection center.

Ex vivo dMRI reveals cortical asymmetry associated with reorganization of connectivity in monkeys injected with *shCRTC1*

We analyzed the *ex vivo* dMRI scans of Monkeys 5 and 6, obtained dMRI connectivity matrices among the whole-cortical supervoxels, and calculated the correlations between the connectivity profiles of the left and right hemispheres as asymmetric for 31 normal marmosets and Monkeys 5 and 6. We found that the *ex vivo* dMRIs of Monkeys 5 and 6 showed increased lateral asymmetry in connectivity, whereas the *ex vivo* dMRIs of the normal marmosets and the *in vivo* dMRI of Monkey 6 tended to show symmetry in most of the connectivity observed before the *shCRTC1* injection (Fig. 7a). We then calculated z scores for the asymmetric features for 39 cortical regions of interest (ROIs). The ROIs that showed significant asymmetry in both Monkeys 5 and 6 were V1, V3, and S1 (Fig. 7b).

In addition, diffusion tensor tractography (DTT) analysis of white matter bundles in the V1-frontal (V1-F; Fig. 7c left) and V1-temporal (V1-T; Fig. 7c right) regions was

performed to compare the number of extracted fiber tracts in the right and left hemispheres. A left-right imbalance of V1-T was observed only in the *ex vivo* MRI of Monkeys 5 and 6 and not in the *ex vivo* MRI of normal marmosets or in the *in vivo* MRI of Monkey 6. In contrast, a left-right imbalance of the V1-F bundle was observed in the *ex vivo* MRI of Monkeys 5 and 6 and even in the *ex vivo* MRI of a normal marmoset and the *in vivo* MRI of Monkey 6 (Fig. 7d). Thus, we observed the structural changes in the whole cortical network of Monkeys 5 and 6 by compared to normal marmoset cortices.

Discussion

We report here that three-site injection of *shCRTC1*#1 into marmoset V1 caused epilepsy that spread throughout the cortex on the unihemisphere with the following time course: (1) Expression of cell death related markers around the injection site. (2) IEG induction spread widely beyond the injection site of shCRTC1# when injected at three sites in V1. (3) Spread of electrical activity throughout the cortex, and (4) formation of lesions at the injection sites and the temporal lobe. We observed neuronal loss, activation of astrocytes and microglia by GFAP and IBA1, respectively, and lesions surrounded by the glial scar. (5) ECoG recordings over the cortex suggested that HFOs

were induced at the *shCRTC1* injection site, spread around it, and eventually propagated throughout the cortex. cwHFOs were induced not only around the injection site, but also gradually from electrodes in the temporal cortex, and eventually more of them originated from the temporal lobe. The association between HFAs and several behavioral outcomes shown in the results confirms that the abnormal neuronal activities induced by three *shCRTC1* injections were indeed epileptic responses, as these associations were observed repeatedly over a month. In Monkey 5, MRI and Nissl staining confirmed tissue lesions in the temporal lobe, suggesting epilepsy focal to the temporal lobe (Figs. 6h and 6i). On the other hand, epilepsy symptoms in this model may go into remission within a few months after injection. Five-month follow-up of monkey 6, from 3 months onwards, the frequency of cwHFOs decreased significantly (Fig. 4f and Extended Data Fig. 10). However, sporadic local HFOs continued to be observed in large areas of the cortex, which were absent in normal marmoset (Extended Data Fig. 10c). This may provide new insights into the relationship between intercortical network reorganization and remission of epilepsy symptoms.

Structural changes long time, several months after, *shCRTC1* injection were evident not only in the histology of the temporal lobe of Monkey 5 (Fig. 6d), but also in the e*x vivo* dMRI-based tractography of both *shCRTC1*#1-injected marmosets (Fig. 7). Analysis of

the correlation between the left-right profiles of the *ex vivo* dMRI connectivity showed lower values in *shCRTC1*#1-injected Monkeys 5 and 6 than in normal marmosets; the lateralization of the V1-F fiber tractography was confirmed by *ex vivo* MRI in normal marmosets and by *in vivo* MRI in Monkey 6. Despite these structural changes, we observed a reduction in cwHFO and stabilization of functional connectivity.

At later stages (2 and 5 months) of the *shCRTC1*#1 injection, activated astrocytes may act as an anti-inflammatory agent with glial scar formation by astroglia, preventing further tissue damage from spreading[26]. It has been reported that activated microglia that appear early after status epilepticus, are required for the induction of epileptogenic astrocytes that appear late after status epilepticus[27]. In our case, when the efficacy of the injected *shCRTC1* was limited by injection size, reduced efficiency of each *shCRTC1*, monocular TTX injection, or a combination of these conditions, activation of astrocytes and microglia appeared even before the induction of IEGs could be detected. Furthermore, strong IBA1 and GFAP signals were observed at the site of *shCRTC1* injection in all subjects. *shCRTC1* injection could eventually cause a situation similar to status epilepticus, but it needs to be confirmed.

A limitation of the current study is the potential off-target effect of *shCRTC1*#1 on epilepsy. However, this is less likely for several reasons despite variations among the

five *shCRTC1*s. Firstly, these *shCRTC1*s are highly selective for the CRTC1 gene in the marmoset genome (see Method, Fig. 3b). Secondly, although *shCRTC1*#2 appears to induce more cell death than #1, they also share similar function of inducing IEG at least to some extent. Moreover, Monkey 7, injected with *shCRTC1*#1 at one site, and *shCRTC1*#2 and #3 at one and two sites respectively, exhibited diffuse IEG expression similar to Monkey1 (Supplementary Table 1).

Based on our observations, we propose a model: *CRTC1* KD induces cell-death signals, followed by aberrant IEG expression (Fig. 8). In addition to the Fig. 8 legend, *de novo* SIK1 mutations cause SIK syndrome, impacting HDAC5, synaptic activity response genes in humans and mice[28-30]. *SIK1* variation disrupts *MEF2*, *Nur77* (NR4A1) and *Neureglin 1* expressions[28]. *Creb* and *Crem* disruption in mice leads to apoptosis in postmitotic neurons and postnatal forebrain, causing hippocampal, striatal neurodegeneration[31]. Correlated roles of *Sirt1*, *Crtc1*, *CREB* in the neuroprotective pathway of mutant mouse huntingtin are reported[32]. Thus, our proposed pathway may suggest a direction, which needs to be proven in future study.

The marmoset epilepsy model based on the current studies may be a notable advance to analyze epilepsy by ECoG and dMRI in real time from the onset of the event. Epilepsy is typically manifested by recurrent seizures and can only be diagnosed at unavoidable

intervals. Unlike previous models which were induced by trauma, infection, ischemia-induced membrane potential changes or brain damage[8], channel genes[33], and mice deficient in all three PAR bZip proteins[34], the *shCRTC1* model uses single gene local KD. This allows to observe the chronological progression of epilepsy, as *shCRTC1* KD marmosets revealed the early mechanisms of epilepsy. This approach could lead to the development of new antiepileptic drugs targeting early-onset epilepsy. It could also be applied to early diagnosis, anticonvulsant prescription and treatment of focal and structural epilepsy, while conventional models maintain the dependence on globally induced brain damage.

Methods

The experimental procedures, including tissue preparation, in situ hybridization (ISH), and IHC, were essentially performed as described or cited in our previous work unless specifically stated otherwise below. The earlier experiments were conducted in accordance with the guidelines of the National Institutes of Health and the Ministry of Education, Culture, Sports, Science and Technology (MEXT) of Japan and were approved by the Animal Care and Use Committee of the National Institutes of Natural Sciences. All other experimental procedures were approved by the Experimental Animal Committee of RIKEN.

shRNA preparation and plasmid construction

Five shRNA sequences were made. *ShCRTC1*#1 and #2 were made from the coding region, and *shCRTC1*#3-#5 were made from the 3'-UTR. BLAST analysis for the authentic marmoset *CRTC1* gene [CREB-regulated transcription coactivator 1 *Callithrix jacchus* (white-tufted-ear marmoset) Gene ID: 100385682, updated on 15-Aug-2022; Ensembl: ENSCJAG00000007421] provided 100% query coverage and an E value of 0.006 for *shCRTC1*#1, #2, #3, #4, and #5, while the lowest E value among all other marmoset genes was >0.05. Identification of *shCRTC1*s with knockdown effects and

degree of efficiency were determined in vitro (see Extended Figure 1), and those having high efficacy were accordance tested more than twice.

AAV vectors for shRNA expression (see Fig. 1a) were based on pAAV-U6-shRNA-2A-hSYNI-hrGFP[35]. A shRNA cassette was inserted into the plasmid digested with BamHI and HindIII located directly below the U6 promoter. To detect the infected cell, hSYNI-hrGFP was replaced Sirius[36] fused human histone H2B (Gene ID: 8970, GenBank ID: X00088) with 3xFlag tag driven by the short version of the mouse CamKIIa promoter. Sirius/pcDNA3 was a gift from Dr. Takeharu Nagai (Addgene http://n2t.net/addgene: plasmid #51957; RRID: Addgene_51957).

AAV injection

Adeno-Associated Viruse serotype 1 was used in all the experiments. They were produced in HEK293 cells using a helper-virus-free system, and purified twice with $CsCl_2$ density gradients and titrated by Q-PCR as described previously[37]. Surgery for shRNA injection was performed as previously described with some modifications[38]. Stereotaxic positions were aligned by using the interaural plane and the anterior border of the cortex. The injection position was determined by the distance from the posterior end of the exposed head bone for the AP direction, and by the distance from the midline

of the skull for the ML direction. All injections were performed in V1 on the cortical surface, and adjacent injection sites were injected 2-3 mm apart in the DM and ML directions, respectively. Pressure injection was performed using a 30 μm outer diameter glass micropipette connected to a nanoliter 2000 injector with a Micro4 controller (World Precision Instruments). To inject AAV into the marmoset V1 cortex, the injector was tilted 30 degrees to the tangent perpendicular line. For exposed cortical areas, we injected 0.1 μl each of vector [$5x10^9$ viral genome (vg)/μl] at two depths (0.3-0.5 and 0.6-1.1 mm from the surface). Since the injector was tilted, the depth was varied according to the position of the injection site, with the aim of delivering AAV to all cortical layers. The injection needle was placed at a shallow level in the cortex, left in place for 2 min, and then an injection of 0.1 μl/2.5 min was delivered. The needle was then advanced further, left in place for 2 min, and a second injection of 0.1 μl/2.5 min was given. After a further waiting 2 min, the needle was removed. In Monkey 3, when *shCRTC1*#1 was injected into the left hemisphere, the glass needle was not aligned with the surface of the brain and it was not injected deeply.

Experimental marmosets and manipulation procedures

A total of 10 adult common marmosets (*Callithrix jacchus*, 14–69 months, both sexes)

were used in this study (Supplementary Table 1). Unless otherwise stated, the marmosets were normally reared (NR) under 12hr light and 12hr dark conditions. Perfusion was performed after the animals had been under the light cycle for more than 6hr. Eight marmosets (Monkeys 2, 3,5,6,7,8,9, and 10) did not receive TTX injections and were therefore visually intact. TTX injection and visual manipulation were performed as described previously[12] with minor modifications. Monkeys 1, 3 and 4 were used for light induction experiments as follows: Monkeys 1 and 4 were kept in the dark for 24–41hr after TTX injection into one eye, followed by LS for 24 min before sacrifice; Monkey 3 was kept in the dark for 24–41hr, followed by LS for 24 min before sacrifice and fixation. Monkeys 5 and 6 were used for ECoG recording after injection of *shCRTC1*#1 at three sites in the right hemisphere, as shown in Supplementary Table 1. The experimental schedule and shRNA injection sites of Monkey 1 are shown in Fig. 1b and Extended Data Fig. 3a, those of Monkey 2 in Fig. 2a and Extended Data Fig. 4a, those of Monkey 3 in Figs. 2b-d, and those of Monkey 4 in Fig. 3a. The injection sites for Monkeys 8, and 10 are shown in Fig. 3h, and Extended Data Figs. 5a and 6a, respectively.

ISH

The ISH method was performed on free-floating sections as previously described[39]. Briefly, brain sections (25 mm) were pretreated with 0.1 M PB, 0.75% glycine/0.1 M PB, and 0.3% Triton X-100/0.1 M PB followed by protease K treatment (5 mg, 37°C, 30 min). After acetylation at RT for 10 min, prehybridization and hybridization were performed at 60-70°C for 1hr and overnight, respectively. Sections were washed with 2x standard saline citrate (SSC)/50% formamide/0.1% N-lauroylsarcosine (NLS), treated with RNase A (20 mg/ml), washed again with 2xSSC/50% formamide/0.1% NLS, and immersed in blocking solution (60 min, RT). For single-color ISH, signals were detected by antibody reaction with anti-digoxigenin (DIG)-AP, Fab fragment (Merck) followed by the nitro blue tetrazolium chloride (NBT)/5-bromo-4-chloro-3-indolyl-phosphate (BCIP) system. For two-color ISH, the DIG probe was detected using an HNPP fluorescent detection kit (11758888001, Merck). The FITC probe was detected as follows. The antibody reaction was performed with Peroxidase-IgG Fraction Monoclonal Mouse Anti-FITC (#200-032-037, Jackson ImmunoResearch Laboratory). The signal was then amplified using a TSA PLUS system (NEL747A001KT, Akoya) and detected with Alexa Fluor 488-conjugated anti-DNP antibody (Molecular Probe). The ISH probes are listed in Supplementary Table 2. The *cFOS*, *ZIF268*, *ARC*, *HTR1B* and *HTR2A* probes and the contents and procedures for each reaction used were

described in our previous publication[39].

Immunohistochemistry (IHC)

IHC was performed using a free-floating section method as previously described. Briefly, brain sections were washed with Tris-buffered saline (TBS). The sections were blocked at RT in blocking buffer containing 5% bovine serum albumin, 0.1% Triton X 100, and 4% normal goat serum in TBS, followed by an antibody reaction with the primary antibody at 4°C for 16-72hr. After the samples were washed with TNT buffer (0.1 M Tris-HCl, pH 7.5, 0.15 M NaCl, 0.1% Tween 20), the secondary antibody reaction was performed at RT for 2hr. For multiple fluorescent labeling, the sections were washed with TNT buffer, mounted on glass slides, and embedded in gelatin. For single-color staining, the sections were labeled with avidin-biotin complex using a Vectastain ABC Elite kit (Vector Laboratories, Burlingame, CA) at RT for 1hr, stained with DAB, and embedded in glass slides. Primary antibodies were TORC1/CRTC1 (C71D11) rabbit mAb (2587, Cell Signaling Technology, Inc.), anti-phospho-CREB (Ser133) antibody, clone 10E9 (05-667, Merck), anti-GFAP antibody (ab7260, Abcam), anti-Iba1 rabbit antibody (019-19741, FUJIFILM Wako), anti-NeuN antibody (MAB377, Merck), and anti-c-Fos rabbit polyclonal IgG antibody (sc-52, Santa Cruz

Biotechnology). Because the fluorescence signal of the Sirius protein in brain sections was weak, the signal was enhanced by antibody staining with anti-GFP chicken antibody (ab13970, Abcam), unless otherwise noted. Secondary antibodies were biotinylated (Jackson ImmunoResearch Laboratories) and fluorophore-conjugated antibodies [CyTM5, CyTM3, CyTM2 (Jackson ImmunoResearch Laboratories), and Alexa Fluor 488 (Molecular Probes).

Cell death assay (TUNEL staining)

TUNEL staining was performed using the *In Situ* Apoptosis Detection Kit (TAKARA BIO INC., Japan) with minor modifications. Briefly, free-floating sections were postfixed in 4% paraformaldehyde (PFA) in PB for 2hr at RT or overnight at 4°C. Sections were sequentially treated with 0.75% glycine, 0.3% Triton X-100, 5 mg/ml protease K (incubated at 37°C for 30 min) and 1% H_2O_2 in phosphate-buffered saline (PBS) (at RT for 30 min). The following procedures were performed according to the manufacturer's protocol. After staining with DAB, the sections were mounted on gelatin-coated slides, and Nissl staining was performed as a counterstain, if required.

Histological data Processing

The histological images were obtained using a digital color camera DP70 (Olympus, Tokyo, Japan) attached to a BX- 51 microscope (Olympus), and an all-in-one microscope (Keyence BZ-X710). After image acquisition of brain sections using microscopes, image contrast was optimized, and false colors were applied using Photoshop CS5 or Photoshop 2022 software (Adobe Systems, San Jose, CA) according to AMED image processing guidelines (https://www.amed.go.jp/content/000078447.pdf). Although the sections for ISH were shrunk, the scale bars in the figures indicate the size of the mounted sections, which were not adjusted for shrinkage.

Large Language Models (LLMs)

We used ChatGPT (https://chat.openai.com) to examine some text sentences, writing only on the draft that were written by the authors. We did not use it for the current data analysis.

ECoG recordings

Whole-cortex 64-channel and 96-channel ECoG arrays (Cir-Tech Inc., Japan) were implanted epidurally in the right hemisphere of 2 monkeys (Monkeys 5 and 6). Ten

electrodes implanted in Monkey 5 were cut during implantation. The implantation procedure has been described in detail previously[22]. At the time of implantation (Monkey 5) or 1 week prior to implantation (Monkey 6), the *CRTC1* KD AAV vector was injected into three sites in V1 of the right hemisphere of the monkeys (Fig. 4a). Longitudinal ECoG recordings and behavioral monitoring were conducted for 2 and 5 months after the AAV injections in Monkeys 5 and 6, respectively. During daily 1-2hr monitoring sessions, the monkeys were seated in a primate chair in a dimly lit room. For the first 20 min of the recordings, we presented sound stimuli used in a previous study[15] to examine auditory evoked responses. ECoG signals were recorded at a sampling rate of 1 kHz per channel by using a Cerebus system (Blackrock Microsystems, USA).

Anatomical localization of electrode contacts

The positions of each electrode contact were identified based on postoperative computed tomography and preacquired T2-weighted MRI. The localization procedure has been described in detail previously (Brain/MINDS data portal; DataID: 4958). Based on the putative cortical areas, we divided the electrodes into seven groups, consisting of V1 and visual (Vis), auditory (Au), temporal (TC), sensorimotor (SM), posterior parietal (PC), and prefrontal areas (FC). Vis was defined as visual areas

excluding V1, the site of KD injections. In all monkeys, the electrode array covered the frontal, parietal, occipital, and temporal cortices (Fig. 4b).

dMRI data acquisition

Ex vivo brains were obtained after transcardial perfusion with 4% paraformaldehyde in 0.1 M phosphate buffer (pH 7.4), the marmoset brains were removed, post-fixed at 4^{o}C for 2-3 days, and transferred to 50 mM phosphate buffer (pH 7.4), and scanned 2-3 days after fixation. All marmoset brains had an *ex vivo* MRI scan (T2w and DWI) before further processing. MRI was performed using a 9.4-T BioSpec 94/30 unit (Bruker Optik GmbH) and a transmit and receive solenoid type coil with a 28-mm inner diameter. To acquire *ex vivo* brain data, the brain was wrapped in a sponge and soaked in a fluorine solution, which showed no signal on MRI, in a plastic container. Vacuum degassing was performed to reduce air bubble-derived artifacts. dMRI data sets were acquired using a spin□echo sequence based on Stejskal-Tanner diffusion[40]. Scanning parameters were as follows: repetition time (TR), 4000 ms; echo time (TE), 28.4 ms; flip angle, 90°; field of view (FOV), 38×38 mm; acquisition data matrix, 190×190; reconstructed image resolution, 0.2 mm (with zero-filling interpolation); slice thickness, 0.2 mm; b-value, 3000 s/mm^2; motion-probing gradient (MPG) orientations, 128 axes; and number of

averages (NA), 2.

Data analysis

Preprocessing. For quantitative analysis, the ECoG signal was cropped to the first 15-min recording of each experimental day. The signals were then rereferenced using a common mean reference (CMR) montage (Extended Data Figs. 7a and 8a). In this process, we rereferenced the signal from each channel to the common mean signal across all channels, from which the channel(s) with a standard deviation greater than 250 mV were excluded. The signals were used to calculate functional connectivity. To extract HFA, we applied a bandpass filter (80 to 200 Hz) to the signal and then calculated the envelope using the Hilbert transform (Extended Data Figs. 7b and 8b).

Detection of cwHFO

We defined an HFO as an HFA greater than the mean plus two times the standard deviation of the HFA across all channels. We then counted the number of electrodes showing HFOs at each time point (Extended Data Figs. 7c and 8c), and an event was marked as a cwHFO if the proportion of electrodes exceeded 50% (=0.5). Marked events with an interevent interval of less than 1 s were merged into one cwHFO. During

some putative cwHFOs, Monkey 5 happened to bite the chair, and it was difficult to separate the biting-related noise from neuronal activity. Therefore, we rejected the events from the putative cwHFOs by using a supervised learning method. We recorded movies from marmosets on seven days (22, 35, 42, 51, 55, 57, and 62 days after KD). Using these movies, we manually distinguished biting events from the putative cwHFOs. We labeled 39 biting events from out of 296 cwHFOs. We then trained a linear support vector machine (SVM) to classify these cwHFOs into biting events and others. We focused on the time-averaged HFA of the 33 electrodes that were stably observed on all experimental days. The SVM was applied to the time-averaged signal for time windows ranging from 0 to 400 ms relative to the onset of the cwHFOs. Note that this time window size was optimized using 10-fold cross validation over the seven days. We found that 94% of the cwHFOs occurred on days when we did not record movies and removed the events labeled as biting events from the following analysis. To investigate which cortical region was the origin of the cwHFO, we calculated the mean HFA for the seven cortical groups in a time window ranging from -250 to 0 ms for each cwHFO (V1, Vis, Au, TC, SM, PC, and FC).

Functional connectivity

We obtained a functional connectivity matrix for each recording by using the correlation coefficient from within 15 min of ECoG signals from each electrode. We then averaged all the matrices and compared them with each daily connectivity matrix to evaluate the daily deviation from the average. To examine the day-to-day stability of the functional connectivity, we calculated (1) correlations among the connectivity matrices on experimental days and (2) the mean functional connectivity within and between regions. Finally, to visualize changes in the connectivity within the KD site (V1) for both monkeys, we calculated the p value of the correlation coefficients within the V1 signals among the experimental days using Fisher's z transformation. The transformed correlation coefficients follow a normal distribution under regular conditions[41].

Spatial interpolation of signals

We spatially interpolated the HFA of each electrode to the surface of the standard marmoset brain, BMA 2019 Ex vivo[42]. We construct the left and right surfaces of the standard brain using iso2Mesh[43], where the number of hemisphere vertices is 1672 and the average distance between the vertices is 1 mm. The interpolated HFA of each vertex at a specific timepoint was calculated using a Gaussian process regression[42] with a 3-dimensional isotropic Gaussian kernel of sigma = 4 mm.

dMRI analysis

We obtained structural connectivity maps based on 36 individual *ex vivo* dMRI scans by using a global tractography method[44]. We used the MRI of a standard brain from the Brain/MINDS portal (https://doi.org/10.24475/bma.4520), whose left and right mid-surface was defined on 167082 vertices. We randomly sampled the 12428 vertices from the original surface and defined corresponding supervoxels on the standard brain. The acquired diffusion-weighted MRI data were analyzed to perform DTT using Mrtrix3 and Diffusion Toolkit software (Massachusetts General Hospital, Boston, MA, USA) [45]. Tractography was performed based on fiber assignments using a continuous tracking algorithm[46]. We obtained a connectivity matrix among the supervoxels to count the number of streamlines through two supervoxels. We focused on the asymmetricity of the convexity pattern between the left and right cortices. By setting two symmetric points on the left and right cortices, we calculated the correlation between the connectivity profiles of each cortex at the two points. A low correlation indicates an asymmetric connectivity pattern at these points (the red region of Fig. 7a). To evaluate the asymmetric feature of the epilepsy-model marmosets, we calculated the z score of the asymmetric connectivity pattern of normal marmosets averaged over brain regions,

which we refer to as the asymmetric feature (AF) in Fig. 7b. Fibers passing through the V1 and frontal areas or the V1 and temporal areas were labeled V1-F and V1-T, respectively. Fibers were counted for each right and left hemisphere. We calculated the asymmetry rates on dMRI as R/(R+L), where R and L correspond to the fiber counts for the right and left hemispheres, respectively.

Data availability

The dMRI and ECoG data of this article will be made available in an online repository, the Brain/MINDS Data Portal with a DOI upon publication.

References

1. Watanabe, S., *et al.* Functional and molecular characterization of a non-human primate model of autism spectrum disorder shows similarity with the human disease. *Nat. Commun.* **12**, 5388 (2021).

2. Schmidt, D. & Sillanpaa, M. Evidence-based review on the natural history of the epilepsies. *Curr. Opin. Neurol.* **25**, 159–163 (2012).

3. Loscher, W. Animal Models of Seizures and Epilepsy: Past, Present, and Future Role for the Discovery of Antiseizure Drugs. *Neurochem Res* **42**, 1873-1888 (2017).

4. Bialer, M. & White, H.S. Key factors in the discovery and development of new

antiepileptic drugs. *Nat Rev Drug Discov* **9**, 68-82 (2010).

5. White, H.S. Preclinical development of antiepileptic drugs: past, present, and future directions. *Epilepsia* **44 Suppl 7**, 2-8 (2003).

6. Depaulis, A., David, O. & Charpier, S. The genetic absence epilepsy rat from Strasbourg as a model to decipher the neuronal and network mechanisms of generalized idiopathic epilepsies. *J Neurosci Methods* **260**, 159-174 (2016).

7. van Luijtelaar, G. & Zobeiri, M. Progress and outlooks in a genetic absence epilepsy model (WAG/Rij). *Curr Med Chem* **21**, 704-721 (2014).

8. Pitkanen, A., *et al*. Epileptogenesis in experimental models. *Epilepsia* **48 Suppl 2**, 13-20 (2007).

9. Loscher, W., Klitgaard, H., Twyman, R.E. & Schmidt, D. New avenues for anti-epileptic drug discovery and development. *Nat Rev Drug Discov* **12**, 757-776 (2013).

10. Berg, A.T., *et al*. Revised terminology and concepts for organization of seizures and epilepsies: report of the ILAE Commission on Classification and Terminology, 2005-2009. *Epilepsia* **51**, 676-685 (2010).

11. Scheffer, I.E., *et al*. ILAE classification of the epilepsies: Position paper of the ILAE Commission for Classification and Terminology. *Epilepsia* **58**, 512-521 (2017).

12. Nakagami, Y., Watakabe, A. & Yamamori, T. Monocular inhibition reveals temporal and spatial changes in gene expression in the primary visual cortex of marmoset. *Frontiers in Neural Circuits* **7** (2013).

13. Uchida, S., *et al.* CRTC1 Nuclear Translocation Following Learning Modulates Memory Strength via Exchange of Chromatin Remodeling Complexes on the Fgf1 Gene. *Cell Rep* **18**, 352-366 (2017).

14. Ch'ng, T.H., *et al.* Activity-dependent transport of the transcriptional coactivator CRTC1 from synapse to nucleus. *Cell* **150**, 207-221 (2012).

15. Komatsu, M., Takaura, K. & Fujii, N. Mismatch negativity in common marmosets: Whole-cortical recordings with multi-channel electrocorticograms. *Sci Rep* **5**, 15006 (2015).

16. Kaneko, T., Komatsu, M., Yamamori, T., Ichinohe, N. & Okano, H. Cortical neural dynamics unveil the rhythm of natural visual behavior in marmosets. *Commun Biol* **5**, 108 (2022).

17. Jiang, Y., *et al.* Constructing the hierarchy of predictive auditory sequences in the marmoset brain. *Elife* **11** (2022).

18. Watakabe, A., *et al.* Comparative analysis of layer-specific genes in Mammalian neocortex. *Cereb Cortex* **17**, 1918-1933 (2007).

19. Paxinos, G., Watson,C., Petrides, M., Rosa, M., Tokuno, H. *The maomoset brain in sterotaxic coordinates.* (Academic Press, Elsevier, Amsterdam, Boston, Heidelberg,London, New York, Oxford, Paris, San Diego, San Francisco, Singapore, Sydne, Tokyo, 2012).

20. Nonaka, M., *et al.* Region-specific activation of CRTC1-CREB signaling mediates long-term fear memory. *Neuron* **84**, 92–106 (2014).

21. Burnos, S., *et al.* Human intracranial high frequency oscillations (HFOs) detected by automatic time-frequency analysis. *PLoS One* **9**, e94381 (2014).

22. Komatsu, M., Kaneko, T., Okano, H. & Ichinohe, N. Chronic implantation of whole-cortical electrocorticographic array in the common marmoset. in *J Vis Exp* (2019).

23. Kaneko, T., Komatsu, M., Yamamori, T., Ichinohe, N. & Okano, H. Cortical neural dynamics unveil the rhythm of natural visual behavior in marmosets. *Commun. Biol.* **5**, 108 (2022).

24. Jacobsen, S.C., *et al.* Effects of short-term high-fat overfeeding on genome-wide DNA methylation in the skeletal muscle of healthy young men. *Diabetologia* **55**, 3341–3349 (2012).

25. Jirsch, J.D., *et al.* High-frequency oscillations during human focal seizures. *Brain* **129**, 1593–1608 (2006).

26. Xu, S., *et al.* Role of astrocytes in post-traumatic epilepsy. *Front. Neurol.* **10**, 1149 (2019).

27. Sano, F., *et al.* Reactive astrocyte-driven epileptogenesis is induced by microglia initially activated following status epilepticus. *JCI Insight* **6** (2021).

28. Proschel, C., *et al.* Epilepsy-causing sequence variations in SIK1 disrupt synaptic activity response gene expression and affect neuronal morphology. *Eur. J. Hum. Genet.* **25**, 216–221 (2017).

29. Hansen, J., *et al.* De novo mutations in SIK1 cause a spectrum of developmental epilepsies. *Am. J. Hum. Genet.* **96**, 682–690 (2015).

30. Pang, B., *et al.* An epilepsy-associated mutation of salt-inducible kinase 1 increases the susceptibility to epileptic seizures and interferes with adrenocorticotropic hormone therapy for infantile spasms in mice. *Int. J. Mol. Sci.* **23**, 7927 (2022).

31. Mantamadiotis, T., *et al.* Disruption of CREB function in brain leads to neurodegeneration. *Nat Genet* **31**, 47-54 (2002).

32. Jeong, H., *et al.* Sirt1 mediates neuroprotection from mutant huntingtin by activation of the TORC1 and CREB transcriptional pathway. *Nat Med* **18**, 159-165 (2011)

33. Oyrer, J., et al. Ion Channels in Genetic Epilepsy: From Genes and

Mechanisms to Disease-Targeted Therapies. Pharmacol Rev 70, 142-173 (2018).

34. Gachon, F., et al. The loss of circadian PAR bZip transcription factors results in epilepsy. Genes Dev 18, 1397-1412 (2004).

35. Takaji, M., *et al*. Distinct roles for primate caudate dopamine D1 and D2 receptors in visual discrimination learning revealed using shRNA knockdown. *Sci Rep* **6**, 35809 (2016).

36. Tomosugi, W., *et al*. An ultramarine fluorescent protein with increased photostability and pH insensitivity. *Nat Methods* **6**, 351-353 (2009).

37. Yagi, H., *et al*. Complete restoration of phenylalanine oxidation in phenylketonuria mouse by a self-complementary adeno-associated virus vector. *J Gene Med* **13**, 114-122 (2011).

38. Watakabe, A., *et al*. Local and long-distance organization of prefrontal cortex circuits in the marmoset brain. *Neuron* **111**, 2258-2273 e2210 (2023).

39. Watakabe, A., *et al*. Comparative analysis of layer-specific genes in Mammalian neocortex. *Cereb Cortex* **17**, 1918–1933 (2007).

40. Stejskal, E.O. & Tanner, J.E. Spin diffusion measurements: spin echoes in the presence of a time-dependent field gradient. *J. Chem. Phys.* **42**, 288–292 (1965).

41. Fisher, R.A. Frequency distribution of the values of the correlation coefficient

in samples from an indefinitely large population. *Biometrika* **10.4**, 507–521 (1915).

42. Woodward, A., *et al.* The NanoZoomer artificial intelligence connectomics pipeline for tracer injection studies of the marmoset brain. *Brain Struct. Funct.* **225**, 1225–1243 (2020).

43. Tran, A.P., Yan, S. & Fang, Q. Improving model-based functional near-infrared spectroscopy analysis using mesh-based anatomical and light-transport models. *Neurophotonics* **7**, 015008 (2020).

44. Rasmussen, C.E. & Williams, C.K.I. *Gaussian Processes for Machine Learning* (The MIT Press, Boston, 2006).

45. Wang, R., Benner, T., Sorensen, A.G. & Wedeen, V.J. Diffusion toolkit: a software package for diffusion imaging data processing and tractography. *Proc. Intl. Soc. Mag. Reson. Med.* **15**, 3720 (2007).

46. Mori, S. & van Zijl, P.C. Fiber tracking: principles and strategies - a technical review. *NMR Biomed.* **15**, 468–480 (2002).

47. Shibasaki, F., Price, E.R., Milan, D. & McKeon, F. Role of kinases and the phosphatase calcineurin in the nuclear shuttling of transcription factor NF-AT4. *Nature* **382**, 370–373 (1996).

48. Uchida, S., *et al.* CRTC1 nuclear translocation following learning modulates

memory strength via exchange of chromatin remodeling complexes on the Fgf1 gene. *Cell Rep.* **18**, 352–366 (2017).

49. Ch'ng, T.H., *et al.* Activity-dependent transport of the transcriptional coactivator CRTC1 from synapse to nucleus. *Cell* **150**, 207–221 (2012).

50. Jagannath, A., *et al.* The CRTC1-SIK1 pathway regulates entrainment of the circadian clock. *Cell* **154**, 1100–1111 (2013).

51. Bito, H., Deisseroth, K. & Tsien, R.W. CREB phosphorylation and dephosphorylation: a Ca(2+)- and stimulus duration-dependent switch for hippocampal gene expression. *Cell* **87**, 1203–1214 (1996).

52. Berdeaux, R., *et al.* SIK1 is a class II HDAC kinase that promotes survival of skeletal myocytes. *Nat. Med.* **13**, 597–603 (2007).

53. Kalra, N. & Kumar, V. c-Fos is a mediator of the c-myc-induced apoptotic signaling in serum-deprived hepatoma cells via the p38 mitogen-activated protein kinase pathway. *J. Biol. Chem.* **279**, 25313–25319 (2004).

54. Chen, X., *et al.* Up-regulation of c-Fos associated with neuronal apoptosis following intracerebral hemorrhage. *Cell. Mol. Neurobiol.* **35**, 363–376 (2015).

55. Preston, G.A., *et al.* Induction of apoptosis by c-Fos protein. *Mol. Cell. Biol.* **16**, 211–218 (1996).

Acknowledgements

We thank RIKEN RRD and N. Hasegawa for their support. We also thank Dr. Hirofumi Nakatomi for suggestions on various aspects of epilepsy studies. This work was supported by the Program for Scientific Research on Innovative Areas (grant number, 22123009) from MEXT, Japan, and by the Program for Brain Mapping by Integrated Neuro technologies for Disease Studies (Brain/MINDS: JP15dm0207001 to T.Y. and M.K., JP19dm0207069 to M.K., JP19dm0207088 to K.N.) from AMED. JSPS KAKENHI: JP22H05154 and 22H05163 to K.N.

Author information

Laboratory of Molecular Analysis for Higher Brain Function

Center for Brain Science, RIKEN, Japan

Yuki Nakagami, Misako Komatsu, Masanori Ohtsuka, Akiya Watakabe, Tetsuo Yamamori

Laboratory of Haptic Perception and Cognitive Physiology

Center for Brain Science, RIKEN, Japan

Misako Komatsu, Masanori Ohtsuka, Akiya Watakabe, Tetsuo Yamamori

Central Institute of Experimental Animals, Kawasaki, Japan

Tetsuo Yamamori

Department of Cellular Neuropathology, Brain Science Institute, Niigata University,

Niigata,

Yuki Nakagami

Institute of Innovative Research, Tokyo Institute of Technology, Yokohama, Kanagawa,

JAPAN

Misako Komatsu

Integrated Systems Biology Laboratory Department of Systems Science, Graduate

School of Informatics, Kyoto University; Kyoto, Japan.

Shin Ishi, Ken Nakae

Exploratory Research Center on Life and Living Systems, National Institutes of Natural

Sciences.

Ken Nakae

Brain Image Analysis Unit, RIKEN Center for Brain Science; Wako, Japan.

Junichi Hata, Hideyuki Okano

Keio University School of Medicine, Shinanomachi, Sinjuku-ku, Tokyo, Japan.

Hideyuki Okano

Faculty of Health Science, Tokyo Metropolitan University

Junichi Hata

Division of Genetic Therapeutics, Center for Molecular Medicine, Jichi Medical

University; Shimotsuke, Japan

Hiroaki Mizukami,

Department of Chemistry and Biomolecular Science

Gifu University, Gifu, Japan

Hiroshi Takemori,

Author contributions

Y.N., M.K., K.N., and T.Y. designed the study and drafted the manuscript. Y.N., M.O., and A.W. performed the virus injections and histological studies. H.T. provided the anti-CRTC1 antibody. H.T. , M.O, and A.W. participated in the discussion of CRTC1 function. M.K. established the ECoG system. M.K and Y. N performed the ECoG experiments. M. K. and K.N. analyzed the ECoG and dMRI data. J.H. collected the dMRI data and analyzed the dMRI data. H.M. prepared the AAV vectors. S.I., H.O., and T.Y. supported and supervised the project.

Ethics declarations

This project was supported as stated in the acknowledgement. All authors declare no competing interests.

Figures

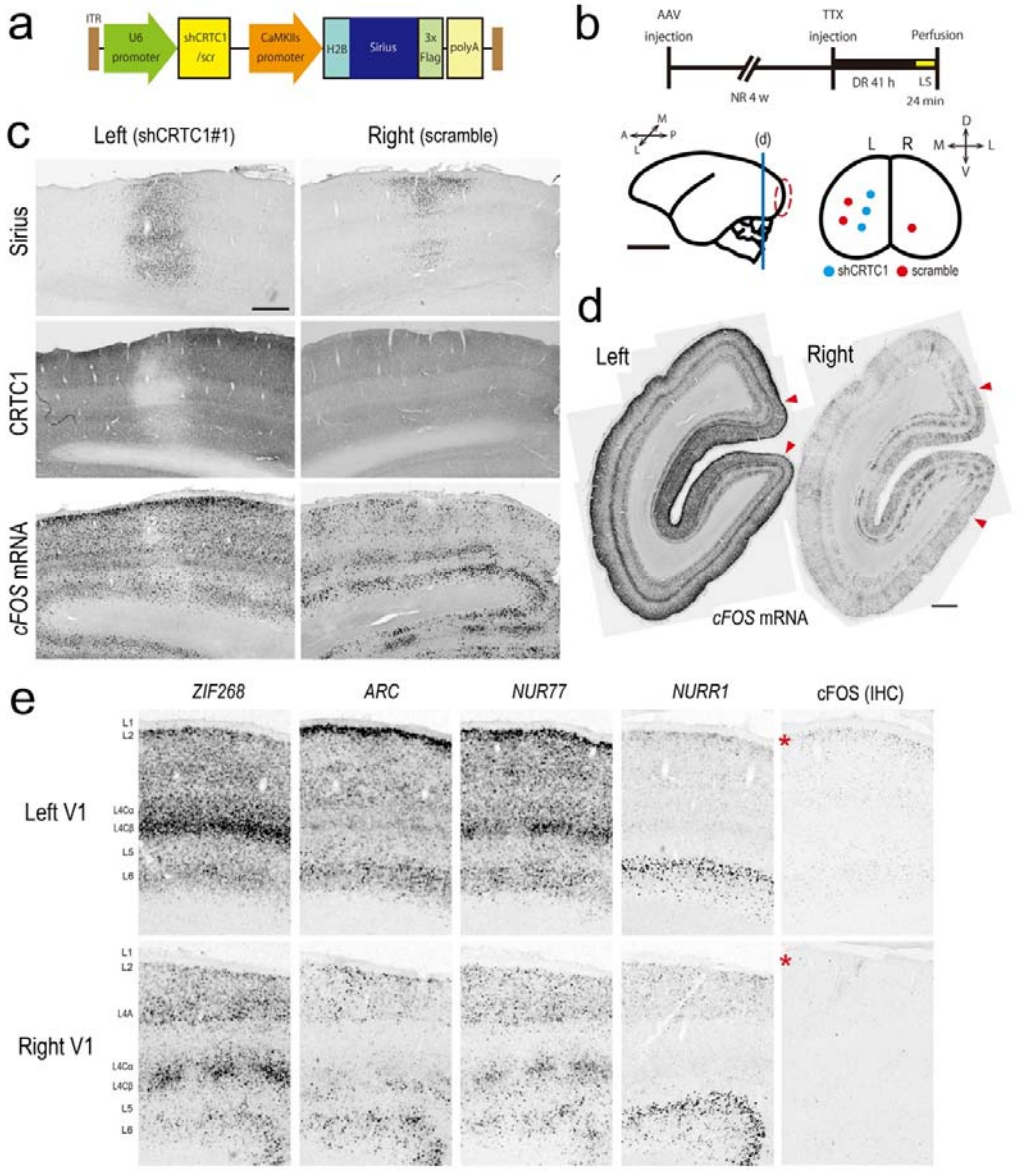

Fig. 1. IEG induction in one hemisphere after injection of *shCRTC1*#l at three sites in Monkey 1. a, Construction *of the* AAV vector encoding *shCRTC1*. ***b***, Upper: The experimental protocol (Monkey 1). Abbreviations: NR (normal rearing), DR (dark rearing), and LS (light stimulation). The time course is from left to right. Lower:

Illustration of the *shCRTC1#1* injection sites. The shRNA was injected into the V1 region indicated by the red dashed circle from the lateral view. The right figure shows the injection site of for *shCRTCI* and *shscr* with red and blue filled circles, respectively. The injection sites in the marmoset V1 are surrounded by the red dotted line (left panel), shown in the posterior view (right panel). Abbreviations: A(anterior), P(posterior), L(lateral), M (medial), D (dorsal), and V (ventral). The blue line under the letters of 'd' marks the position of the coronal plane shown in d. Scale bar (1 cm). **c**, Expression of Sirius (IHC), CRTC1 (IHC), and *cFOS mRNA* (ISH) at the sh*CRTCI*#1 *(left)* and *shscr* (right) injection sites. Scale bar (500 μm). **d**, *cFOS* mRNA expression in coronal sections through the left and right V1. Red arrowheads indicate V1/V2 borders. Scale bar: 1 mm. **e**, Magnified views of the expression of five IEGs in the left and right V1. Sections adjacent to those examined for *cFOS* mRNA expression in Fig. 1d were analyzed. cFOS protein was detected by IHC. Signals for all IEGs except cFOS (far right) are ISH signals. Red asterisks indicate layer 2.

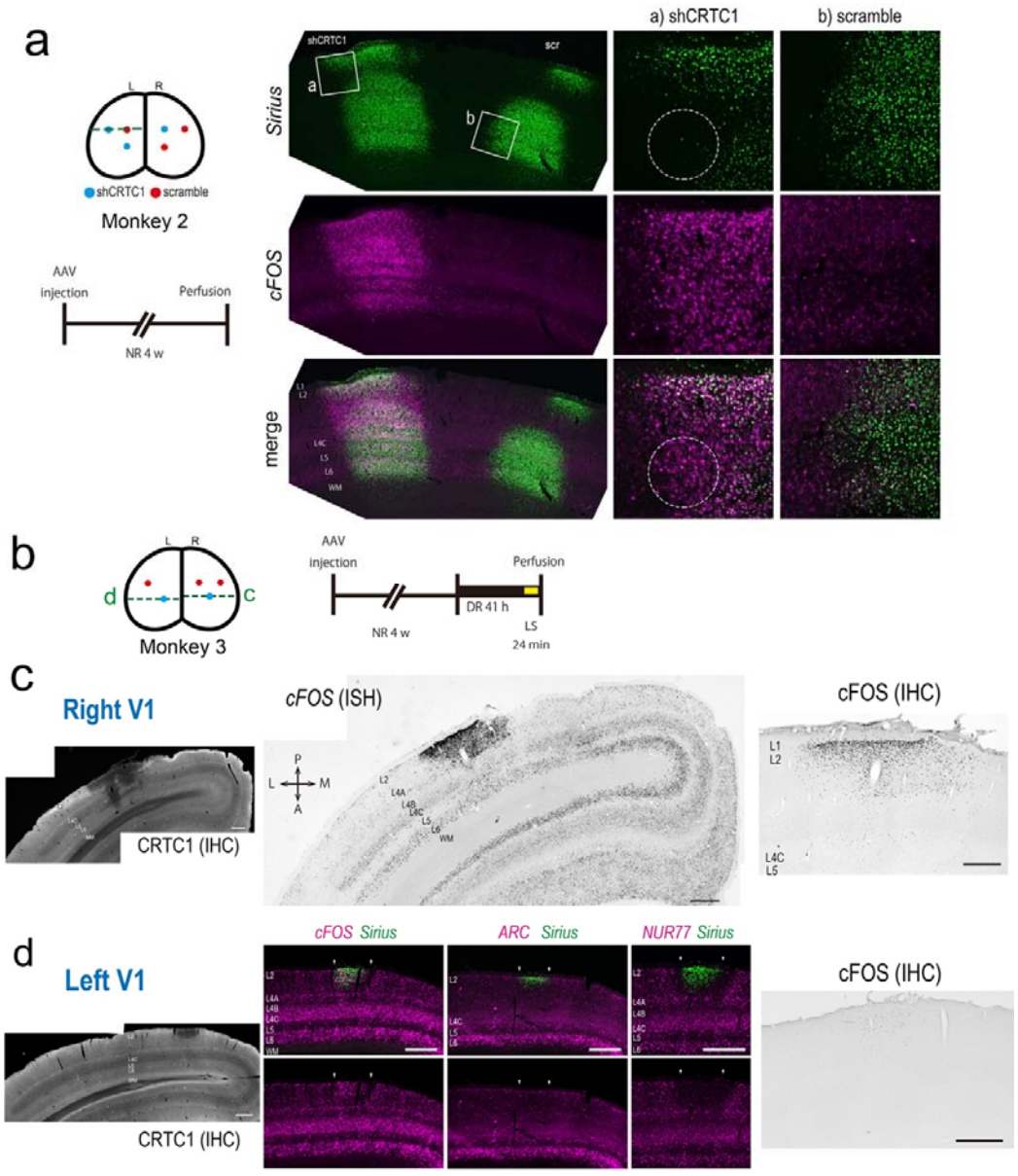

Fig. 2. cFOS expression after injection of *shCRTC1*#1 into one site per hemisphere.

a, Upper left panel: Three injections were made into each hemisphere; two of *shCRTC1*#1 and one of *shscr* into the left (L) hemisphere and one of *sHCRT1*#1 and two of *shscr* into the right (R) hemisphere of a normally reared animal (Monkey 2). Three panels on the right: Top row: Sirius (green) indicates the expression in the AAV-

infected cells. Middle row: *cFOS* (ISH) was detected at the *shCRTC1*#1 injection site but little at the site of the *shscr* injection site. Bottom row: Merged images of *Sirius* and *cFOS*. **b,** Left: *shCRTC1*#1 was injected into one site in each hemisphere, and *shscr* was injected into one site and two sites in the left and right hemispheres, respectively. Right: A normally reared marmoset that underwent 24 min of LS without a TTX eye injection (Monkey 3). **c-d,** Histological analyses of Monkey 3. (c) Left (right V1): CRTC1 expression detected by IHC. Middle: *cFOS* expression (by ISH). Strong and relatively weak *cFOS* expression was observed at the injection site and through the layers, in response to the *shCRTC1* injection and LS, respectively. Right: cFOS expression by IHC. Scale bars (200 μm). (d) (left V1): Left panel: CRTC1 (IHC). Middle panels (from left to right): *cFOS*, *ARC*, *NUR77* (magenta) with Sirius expression (green). Upper row: merged images. Lower row: IEG expressions. Right panel: cFOS (IHC). L2-6 and wm (layers 1-6 and white matter, respectively). Red and blue filled circles in (a) and (b) indicate the injection sites for *shCRTC1*#1 and *shscr* RNAs, respectively. The other abbreviations are the same as in Fig. 1b.

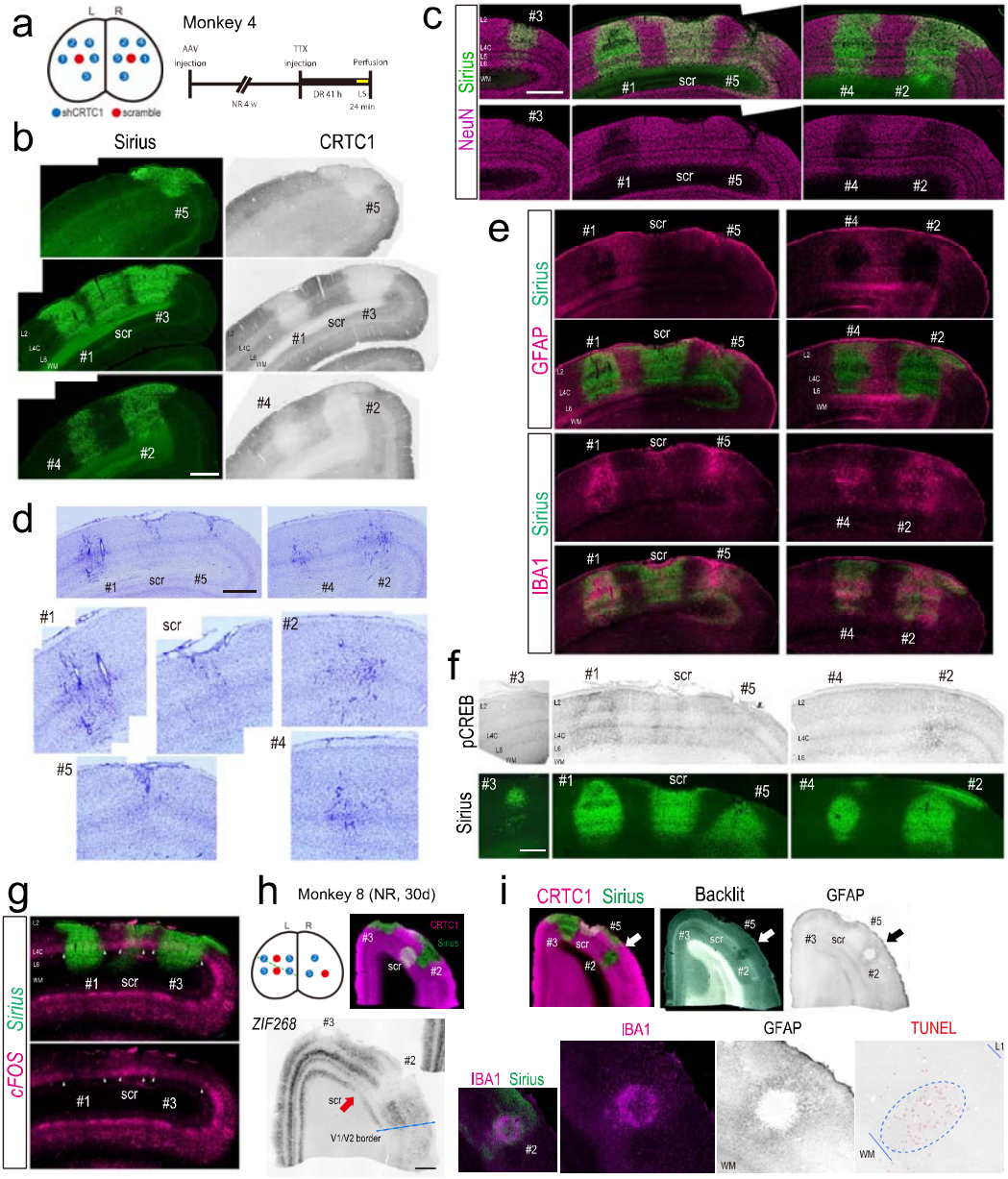

Fig. 3. Expression of cell death related markers and IEGs at each of the *shCRTC1* variant injection site. a, Left: Injection sites of *shCRTC1*#1, #2, #3, #4, #5 (blue circles) and *shscr* (scrambled shRNA, red circles) in Monkey 4 are shown from a posterior view similar to that shown in Fig. 1b. Right: Experimental protocol. **b-g,**

Histological analysis around the injection sites in V1 of Monkey 4. (b) IHC signals of Sirius (left) and CRTC1 (right). Adjacent sections were analyzed. Top: *shCRTC1*#5, middle: *shCRTC1*#1, *shscr* and *shCRTC1*#3, bottom: *shCRTC1*#2 and *shCRTC1*#4. Scale bars (1 mm). (c) Double IHC of NeuN (magenta) and Sirius (green). Top: Merged images of NeuN and Sirius signals. Bottom: NeuN signals. Left column: *shCRTC1*#3, middle column: *shCRTC1*#1, *shscr* and *shCRTC1*#5, right column: *shCRTC1*#4 and *shCRTC*#2, left and right, respectively. Scale bars (1 mm). (d) Nissl stained sections. Top left row: *shCRTC1*#1, *shscr*, and *shCRTC*#5 (from left to right). Top right row: *shCRTC1* #4 and #2 (left and right, respectively). Middle row: enlarged *shCRTC1*#1, *shscr* and *shCRTC*#2 (from left to right). Bottom: *shCRTC1*#5 and #4 (left and right, respectively). Scale bars (1 mm). (e) Double IHC of glial markers and Sirius. Top two panels: GFAP (magenta), Sirius (green). Bottom two panels: IBA1 (magenta), Sirius (green). Nissl staining (d) was performed on the same sections, which were immunostained for IBA1 and Sirius. The IBA1 signal at shCRTC1#5 is due to the trace of the glass needle during injection. (f) Top: Expression of pCREB at each injection site for from *shCRTC1*#1 to *shCRTC1*#5. Bottom: Sirius. Adjacent sections were analyzed. Scale bar (500 μm). (g) Double ISH of *cFOS* (magenta) and *Sirius* (green). Top: merged images. The injection sites of *shCRTC1*#1 (left), *shscr* (middle), *shCRTC1*#3 (right).

Bottom: *cFOS* expression (magenta); arrowheads indicate the borders of each injection. Note that sections of (b) and (g) were obtained from the L hemisphere and sections from (c) to (f) were obtained from the R hemisphere. Adjacent sections were used for (c) to (f). (h) Top left: an illustration of the injection sites of Monkey 8 in the same style as in (a). Green dotted line of L hemisphere: the direction of sectioning. Top right: merged image of double IHC of Sirius and CRTC1 (injection sites: *shCRTC1*#3, *shscr* and #2, left, middle and right, respectively). Bottom: ISH of *ZIF268*, corresponding to the upper right section. The red arrow indicates the position of *shscr* injection site. Blue dotted line shows V1/V2 border. Scale bar (500 μm). (i) Upper three panels (from left to right). Left: merged image of double IHC images of CRTC1 and Sirius (injection sites: *shCRTC1*#3, *shscr*, *shCRTC1* #5 and #2, from left to right). Middle: Backlit image. Right: IHC of GFAP. Bottom Left two panels: Enlarged IHC images of merged of IBA1 and Sirius (left), and IBA1 (right) at the *shCRTC1*#2 injection site. Bottom right two panels: GFAP (left). TUNEL staining (right): The *shCRTC1#2*-injected area is surrounded by the thin blue line. TUNEL signals are marked with small red dots within this blue line. White and black arrows in the upper panels indicate the same injection site of *shCRTC1#2*. Abbreviations: L1 (layer 1), WM (white matter). Scale bars (1 mm).

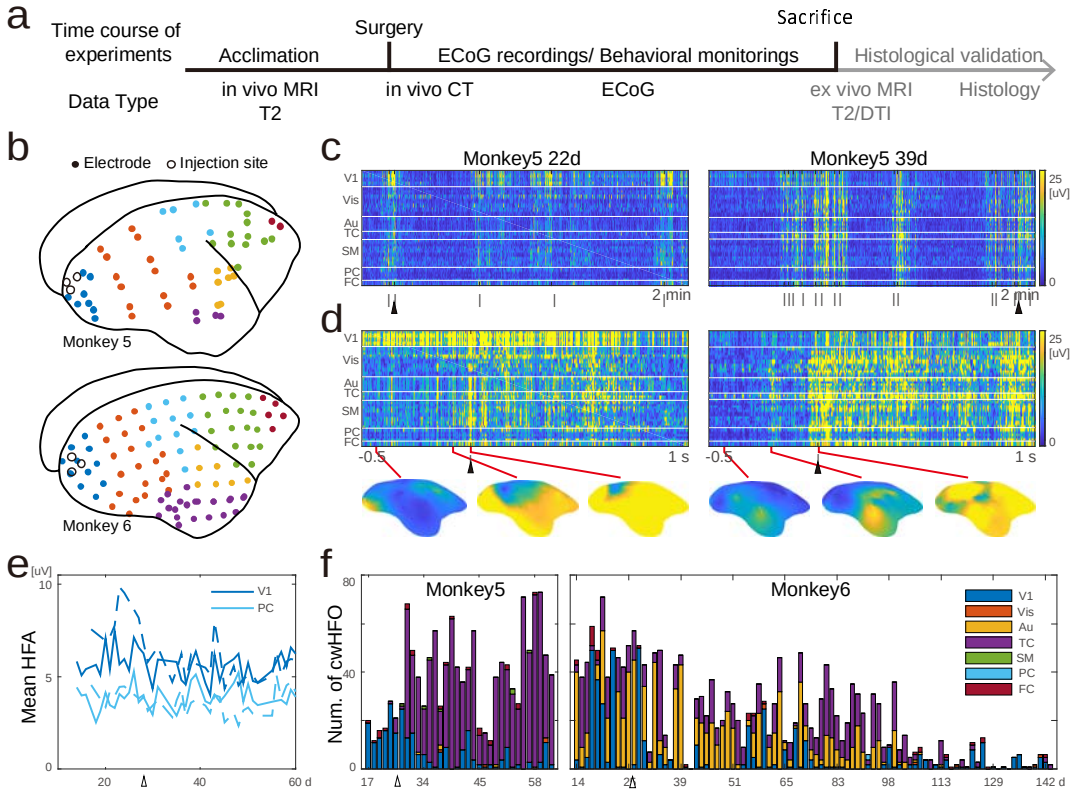

Fig. 4. Local *CRTC 1*KD induced both local and cortex-wide HFOs. a, Time course of the experiments. **b**, Locations of the *shCRTC1*#1 injection sites (open circles) and ECoG electrodes (colored dots) in Monkeys 5 and 6. The colors of the dots indicate the grouped cortical regions: V1, Vis, Aud, TC, SM, PC, and FC. The color code is the same as shown in the inset of (f). **c**, Examples of HFA (80-200 Hz) in Monkey 5. The vertical bars at the bottom of the figures indicate the onset of cwHFOs. The filled triangles correspond to the cwHFO onset magnified in d. **d**, Examples of cwHFOs followed by HFOs in V1 (left) and TC (right). **e**, Mean HFA during 15-min recordings in V1 (blue) and PC (cyan) for each experimental day. The open triangle below the

horizontal axis indicates 28 days after *shCRTC1* knockdown. **f**, Number of cwHFOs for each experimental day. The color of each bar indicates the cortical region that showed the highest HFA from -250 to 0ms before the onset of cwHFO.

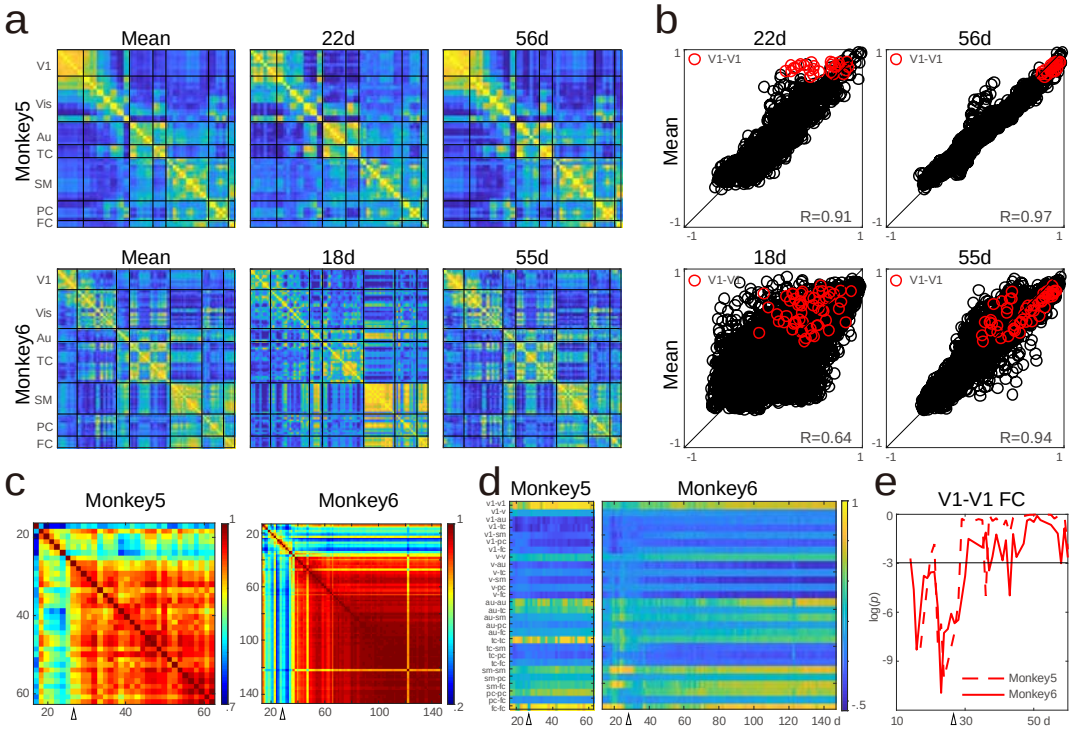

Fig. 5. Altered functional networks reorganized 5 weeks after KD with shCRTC1#1.

a, *CRTC1* KD induced alterations in functional networks. The left columns show the means of the correlation matrices of ECoG signals for Monkeys 5 (top) and 6 (bottom). Middle and right columns are the correlation matrices obtained three (22 days) and eight (56 days) weeks after KD, respectively. The color scale is the same as in d. **b**, Deviation from the averaged functional connection. Each functional connection is plotted on the x-axis for each experimental day and on the y-axis for the averaged network in a. **c**, Stability of functional connections. The left and right figures are the correlation matrices of the functional connections for each experimental day for Monkeys 5 and 6, respectively. The open triangles on the horizontal axis indicate 28 days after *CRTC1*

knockdown. **d**, Functional connections between and within regions. **e,** Transient reductions in functional connectivity (FC) within V1. The horizontal line indicates the one-sided 5% significance level.

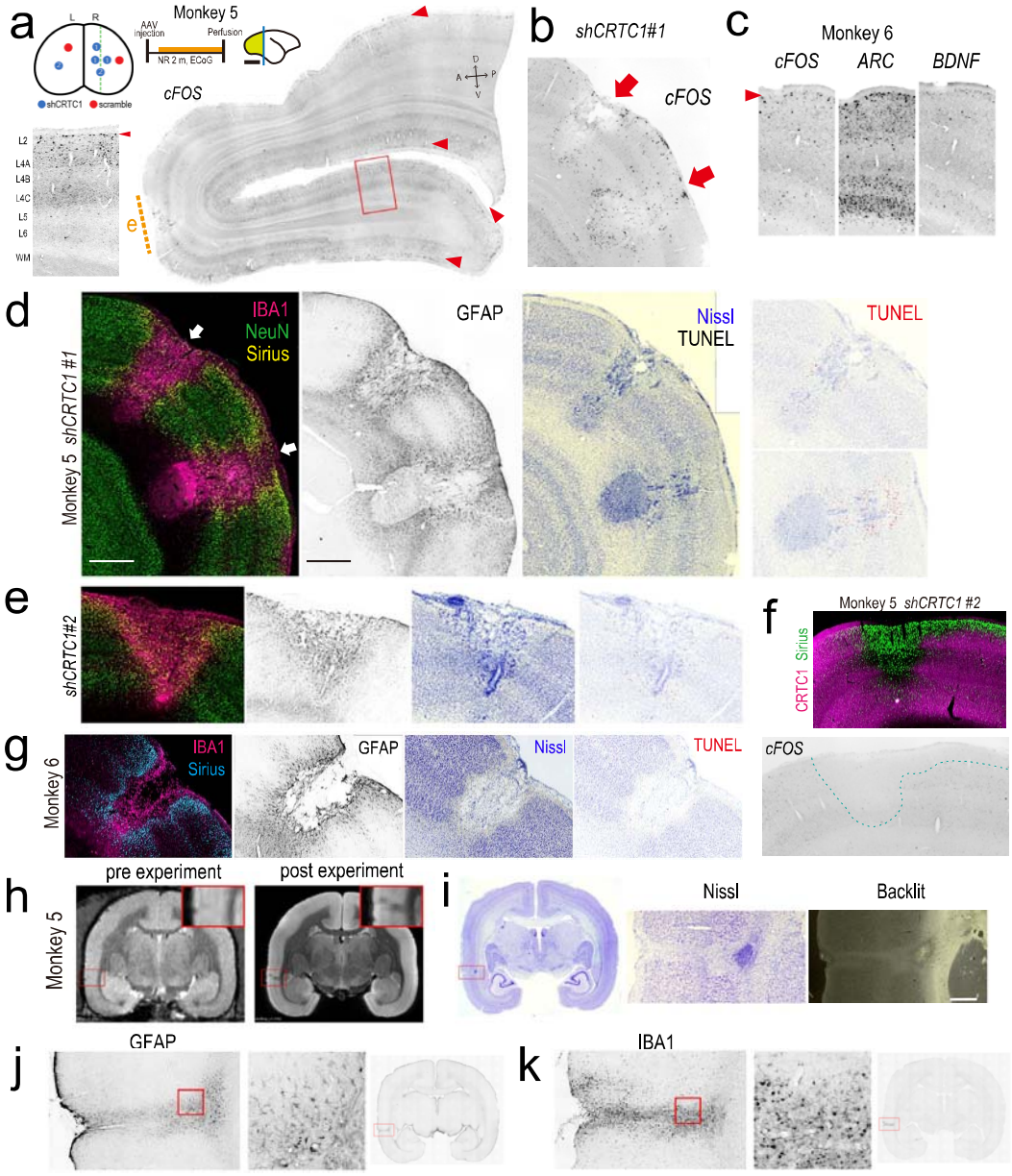

Fig. 6. Histological analysis 63 and 148 days after sh*CRTC1* injection. a, Expression analysis of *cFOS* mRNA in a sagittal section of the right occipital lobe of monkey 5. Left upper three small figures: Left (posterior view showing injection sites), injection sites of *shCRTC1*#1 (blue circles: three sites in the right hemisphere), *shCRTC1*#2 (blue

circles: one site for each hemisphere) and *shscr* (red circles: one site for each hemisphere). Middle: Experimental time course. Right: schematic diagram showing the location of the section. Scale bar: 1 cm. The dotted green line (left; coronal view) and the yellow green area (right; sagittal view) indicate the position of the section. Bottom left: *cFOS* expression from the magnified view in the right section. Right: The large sagittal section shows the full view of the coronal section along with the blue line above. Red arrowheads indicate *cFOS* expression in layer 2. Orange dashed line "e" shows the position shown in Fig. 6e. **b,** Distribution of *cFOS* expression at injection sites of *shCRTC1#1* in Monkey 5. This section is the adjacent section of Fig. 6d. Red arrows indicate the *shCRTC1*#1 injection site, the same position as indicated by white arrows in Figure 6d. **c,** IEG expression in V1 distant from the injection sites in monkey 6: left (*cFOS*), middle (*ARC*), right (*BDNF*). The red arrowhead indicates layer 2. **d-g,** The marmosets were histologically analyzed 63 and 148 days after the *shCRTC1*#1 injections at three sites (Monkey 5 and Monkey 6, respectively; see also Supplementary Table 1). (d) Monkey 5, injected with *shCRTC1*#1 at two injection sites (top left), was analyzed as shown in each of the four columns [IBA1, NeuN, and Sirius; GFAP only; Nissl and TUNEL; and TUNEL signals are displayed in red, from left to right]. Scale bar (500 μm). (e) Monkey 5, injected with *shCRTC1*#2 in the same staining as d.

Adjacent sections with **a** were analyzed. (f) Expression pattern of *cFOS* at *shCRTC1*#2 injection site in Monkey 5. Upper: Merged image of double IHC of CRTC1 and Sirius. Bottom: ISH of *cFOS*. (g) Monkey 6 in the same staining as (d) without NeuN staining. **h**, *In vivo* (left) and *ex vivo* MRI (right) images of Monkey 5. The lesion in the temporal cortex (presumably TE3) is magnified in the upper right inset of each image. **i,** Images of Nissl staining with low magnification (left), high magnification (middle) and "backlit" light microscopy (right). **j,** Three left panels: GFAP signals. Left: the red boxed region of the left images in (i). Middle: High magnification of the region indicated by the red box in the left image. Right: A lower magnification view of the section. **k,** IBA1 signals shown in the same order as the GFAP signals in (j). Adjacent sections were analyzed in (i) and (j).

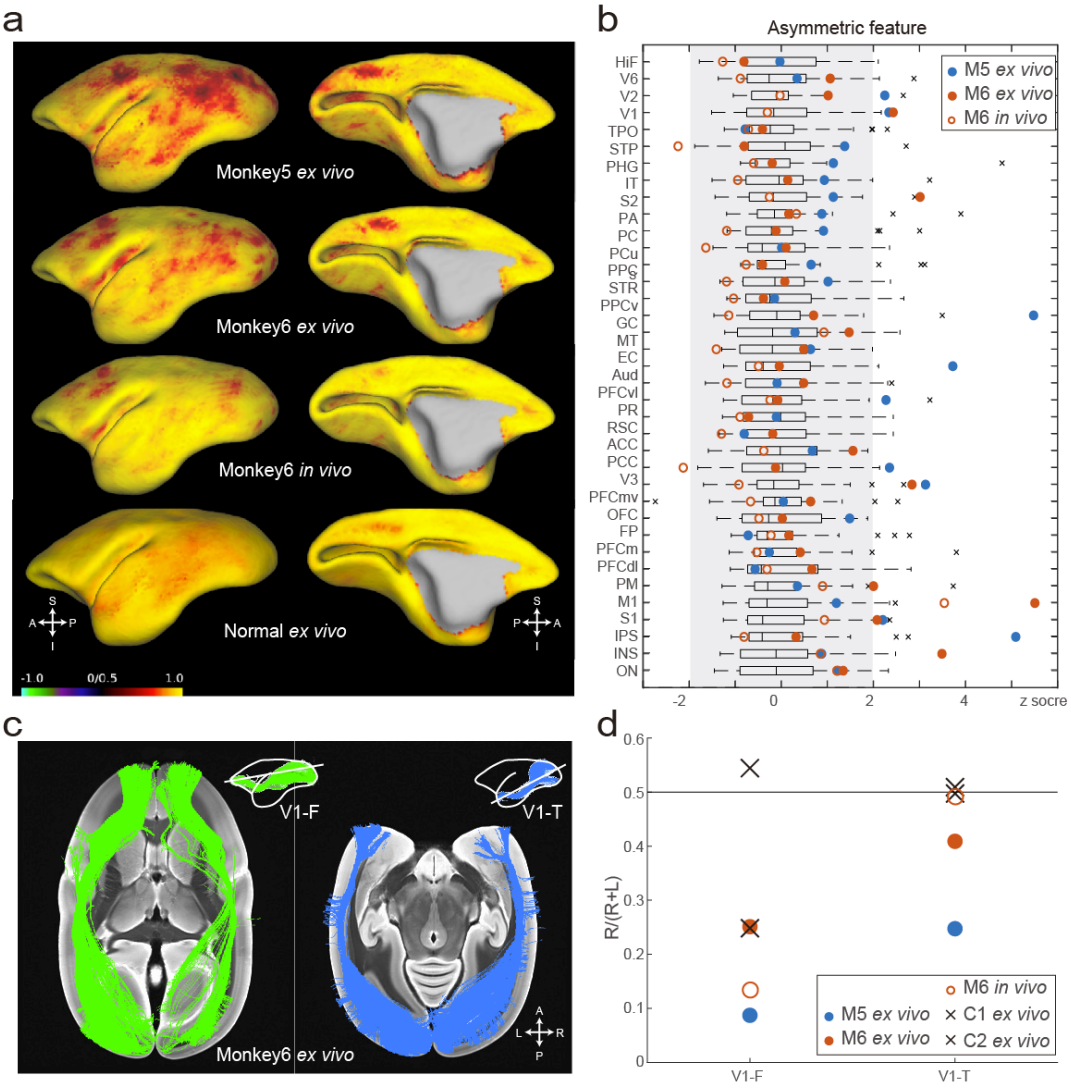

Fig. 7. Postinjection dMRI shows cortical asymmetry. a, Correlations between the left and right profiles of dMRI connectivity at each supervoxel. The red region represents a low correlation, indicating asymmetric connectivity between the left and right cortices. **b**, The asymmetric feature (AF) values of 31 cortical ROIs. Box plot shows the AF from the *ex vivo* dMRI scans of 36 normal marmosets. The gray region represents a significant two-sided z score at a threshold of $p<0.05$ ($-1.96 < z < 1.96$).

Postinjection *ex vivo* AF of Monkey 5, the postinjection *ex vivo* AF of Monkey 6, and postinjection *in vivo* AF of Monkey 6 are indicated as filled blue, filled red, and open red circles, respectively. **c,** Diffusion tensor tractography. Fiber tracts connect V1 and the frontal (left) and temporal (right) areas of Monkey 6. **d**, Asymmetry of the fiber tracts. Abbreviations: HiF=hippocampal formation; V6=visual area 6; V2=visual area 2; V1=primary visual area; TPO=temporopolar area; STP=superior temporal polysensory cortex; PHG=parahippocampal gyrus; IT=inferior temporal area; S2=secondary sensory area; PA = area prostriate; PC=piriform cortex; PCu=precuneus; PPC=postal parietal area; S=subiculum; STR=superior temporal rostral area; PPCv=ventral postal parietal area; GC=gustatory cortex; MT=mid-temporal area; EC=entorhinal cortex; Aud=auditory cortex; PFCvl=ventral lateral prefrontal cortex; PR=perirhinal cortex; RSC=retrosplenial cortex; ACC=anterior cingulate cortex; PCC=posterior cingulate cortex; V3=visual area 3; PFCvm=ventromedial prefrontal cortex; OFC=orbitofrontal cortex; FP=frontal pole; PFCm=medial prefrontal cortex; PFCdl=dorsolateral prefrontal cortex; PM=premotor cortex; M1=primary motor area; S1=primary sensory area; IPS=intraparietal sulcus; INS=insular cortex; ON=olfactory nucleus; OB=olfactory bulb.

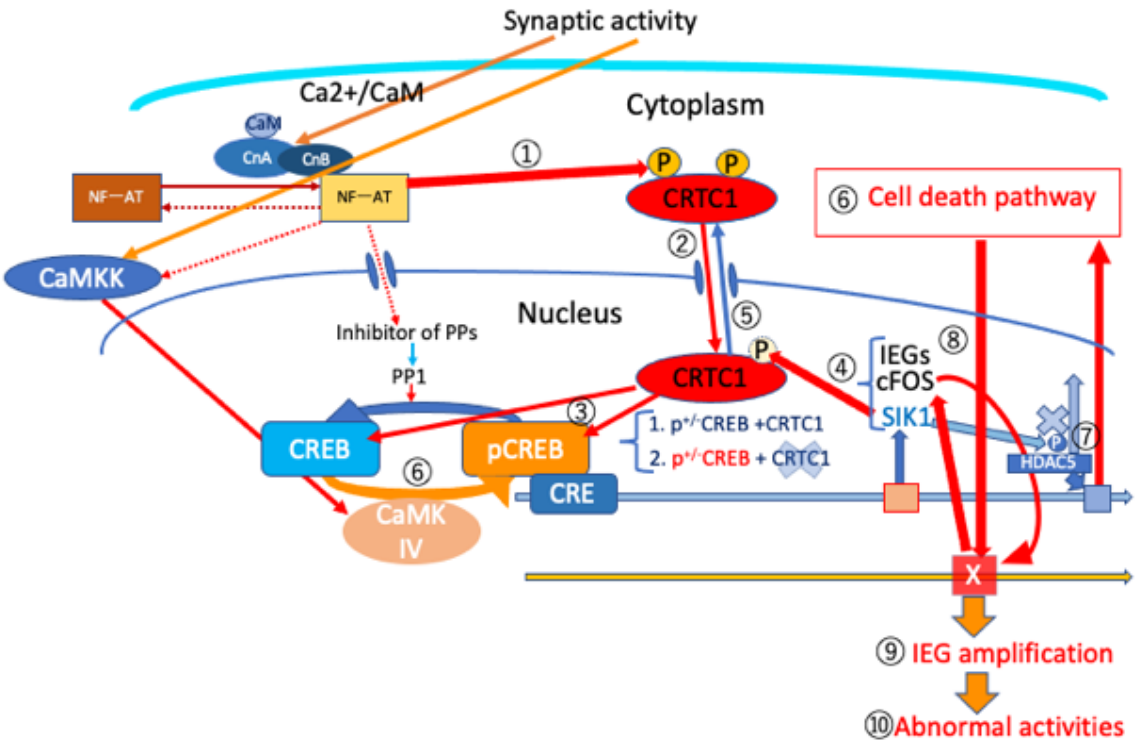

Fig. 8. Model for cell death and IEG induction by *shCRTC1*. We propose a model that explains how *shCRTC1* KD causes cell death signaling. ① Synaptic activity causes Ca2+/calmodulin (CaM) dephosphorylation of CRTC1 mediated by calcineurin (Cn) and NF-AT4[47]. ② Dephosphorylated CRTC1 is transported to the nucleus[20, 48-50]. ③ In the nucleus, CRTC1 activates both phosphorylated and dephosphorylated CREB[20]. ④ CRTC1 and the CREB complex activate SIK1 transcription, whose expression then activates the phosphorylation of CRTC1[20]. ⑤ The phosphorylation of CRTC1 leads to its export to the cytoplasm[20]. Note that there are two parallel pathways that activate the

CREB-dependent cre promoter[20] and thereby control IEGs, including *cFOS* and *SIK1*. ⑥ One is likely to depend on CaM kinase (CaMKK) and CaMKIV-dependent CREB phosphorylation[51]. The other is CRTC1- dependent CREB phosphorylation[20] (③). Either phosphorylated CREB or nonphosphorylated CREB can activate cre dependent IEG expression together with CRTC1[20], both of which pathways are thought to be reduced by *CRTC1* KD. ⑦ A few reports have implicated SIK1 in epilepsy [28-30]. SIK1 is a class II HDAC kinase and promotes skeletal myocyte survival[52]. ⑧ Upregulation of *cFOS* expression with neuronal apoptosis[53, 54] and induction of apoptosis by cFOS have been reported[55]. ⑨ Apoptosis/cell death and the induction of IEGs may cause self-amplification. ⑩ The abnormal expression of IEGs then causes abnormal activities that spread outside the cell.

Extended data

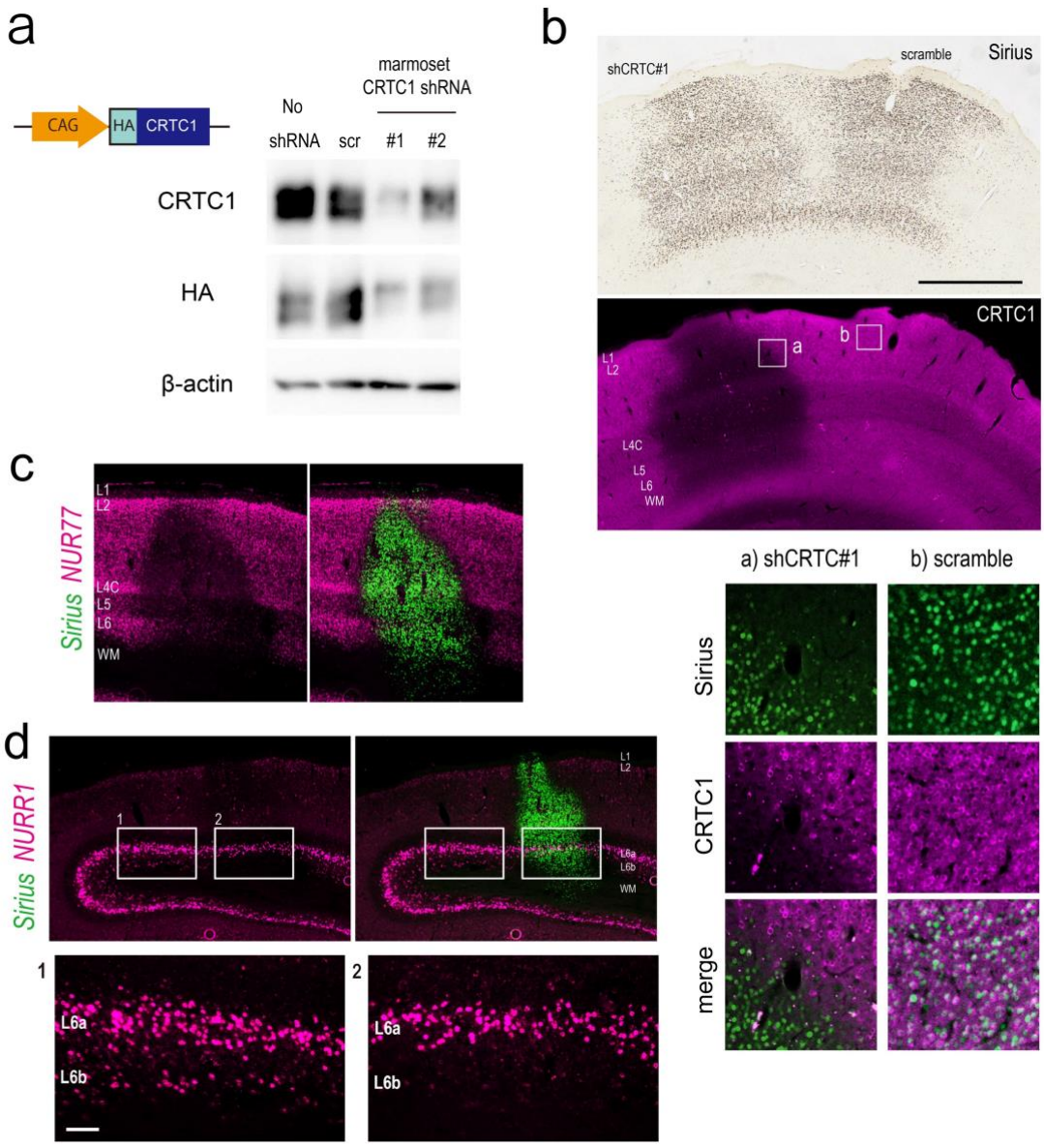

Extended Data Fig. 1. *shCRTC1* construction and its effect on Nurr77 (continued from Fig. 1). a, Construction of an expression vector for the marmoset *CRTC1* gene (left). Western blot (WB) analysis (right). The specificity of *shCRTC1*#1 and #2 was examined by cotransfecting each of the *shCRTC1*s together with the marmoset *CRTC1*

gene into 293T cells. Each WB column shows cotransfection with no shRNA, *shscr*, *shCRTC1*#1, and s*hCRTC1*#2 (from left to right). Each row shows detection with anti-CRTC1, anti-HA and anti-b-actin (from top to bottom). **b,** Top two rows: IHC analysis at the *shCRTC*#1 and *shscr* injection sites in marmoset V1 detected with anti-Sirius (GFP) antibody (top) and CRTC1 antibody (bottom). Adjusted sections were analyzed. Scale bar (1 mm). The bottom three right rows are magnified views of the white square regions (a and b in the small white boxes) in the CRTC1 section, showing Sirius fluorescence, anti-CRTC1 IHC signals, and merged images (top, middle, and bottom rows, respectively) at the *shCRTC*1#1 and *shscr* injection sites (right and left columns, respectively). **c,** Images from ISH analysis showing the *NURR77* signal alone and merged with the Sirius signal (from left to right) at the *shCRTC1*#1 injection site. Layers 1, 2, 4C, 5, 6 and white matter are shown (L1, L2, L4C, L5, L6, and WM, respectively). **d,** ISH analysis of *NURR1* with *Sirius*. Top: *NURR1* alone and merged with *Sirius* (from left to right) at the *shCRTC1*#1 noninjection and injection sites indicated by white boxes 1 and 2, respectively. Layers indicated by L1, L2, L6a and L6b. Bottom: Enlarged views of the above white boxes (box 1, left, and box 2, right) showing layers 6a (L6a) and 6b (L6b). Scale bar (100 μm).

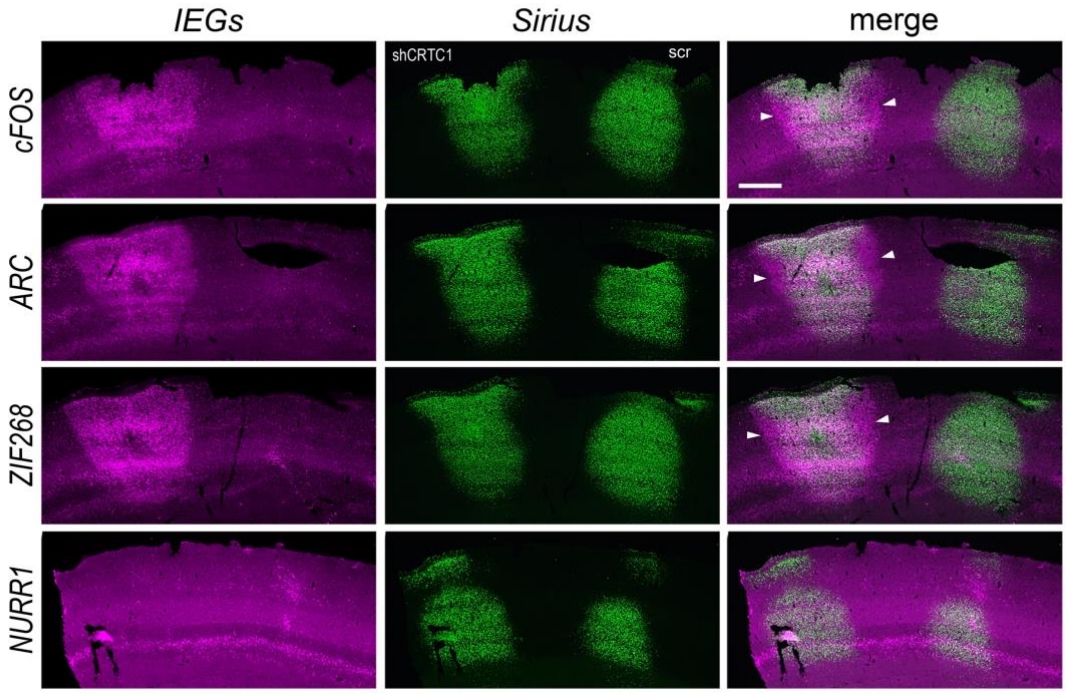

Extended Data Fig. 2. IEG expression around *shCRTC1* and shscr injection sites.

Left column: Four IEG expression patterns were examined around the *shCRTC1* and *shscr* injection sites in Monkey 1. Middle column: Sirius ISH. Right column: Merged images of the IEG and Sirius signals. Rows from top to bottom: *cFOS*, *ARC*, *ZIF268*, and *NURR1* expression by ISH. Arrowheads indicate the border of each IEG expression. Scale bar: 500 μm.

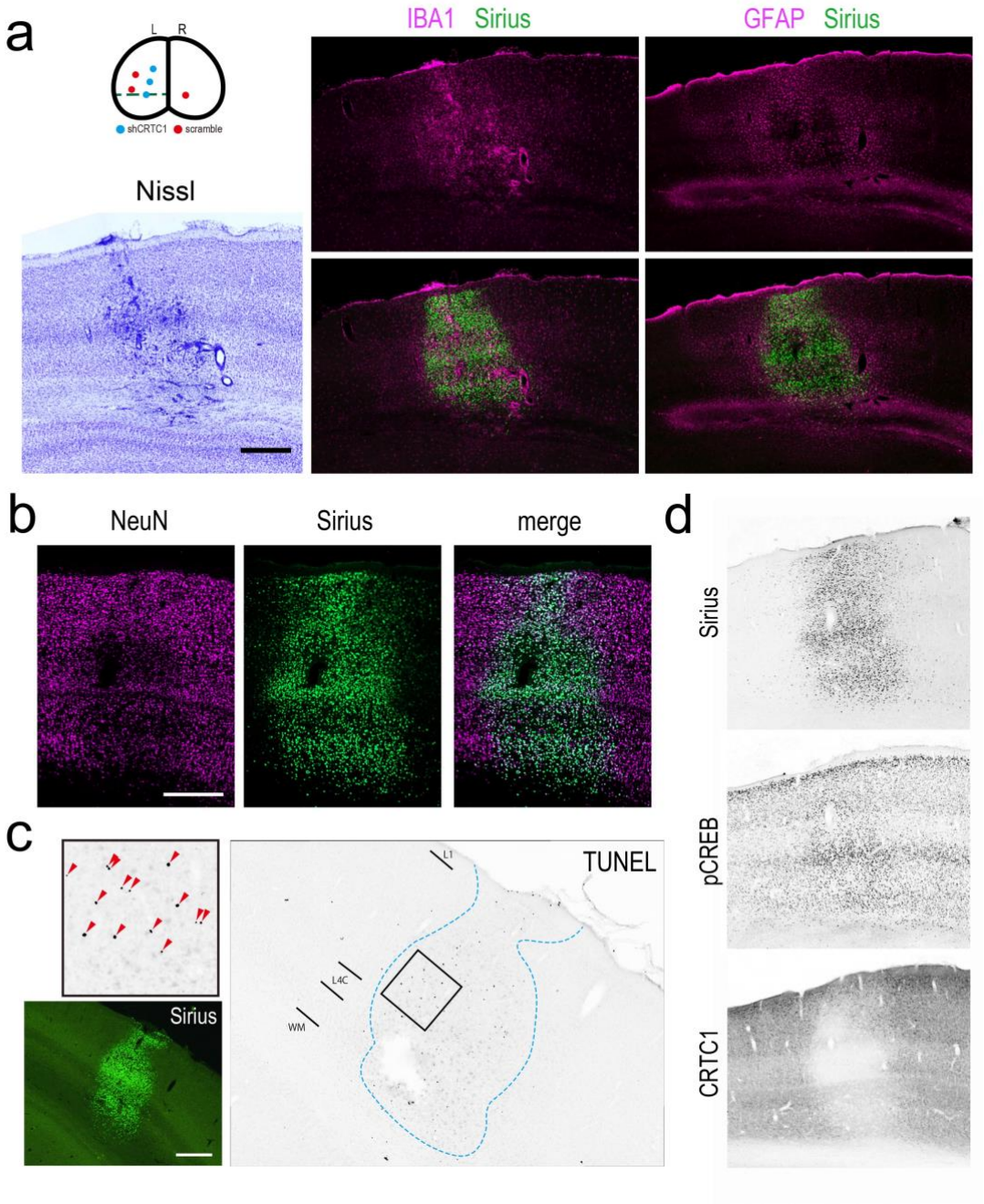

Extended Data Fig. 3: Neuronal, glial and cell death markers around the shRNA injection site in Monkey 1. a, Top left: Illustration of the injection sites. The cross-section, as shown by the dotted line, which includes the *shCRTC1*#1 and *shscr* injection sites, was analyzed histologically. Bottom left: Nissl staining around an injection site.

Histological analysis of Nissl, glial, neuronal and cell death markers. Middle and right panels: Double IHCs of glial markers and Sirius. IBA1 (middle column) and GFAP (right column) signals are shown in magenta. Sirius (green) was used for injection site detection. Adjusted sections were analyzed. Nissl staining was performed on the same section as IBA1 immunostaining. Scale bar 500 μm. **b**, Left and middle: NeuN and Sirius staining are shown in magenta and green, respectively. Right: merged images. Scale bar 200 μm. **c,** TUNEL staining at the injection site. Top left panel is an image of the boxed region of the right panel (enlarged TUNEL-stained region). Bottom left: Sirius. Scale bar 500 μm. Right: Low-magnification view of the *shCRTC1*-injected region. **d,** Top and middle: Sirius expression and phosphorylated CREB signals, were detected at the *shCRTC1* injection site, respectively. Bottom: CRTC1 expression (IHC).

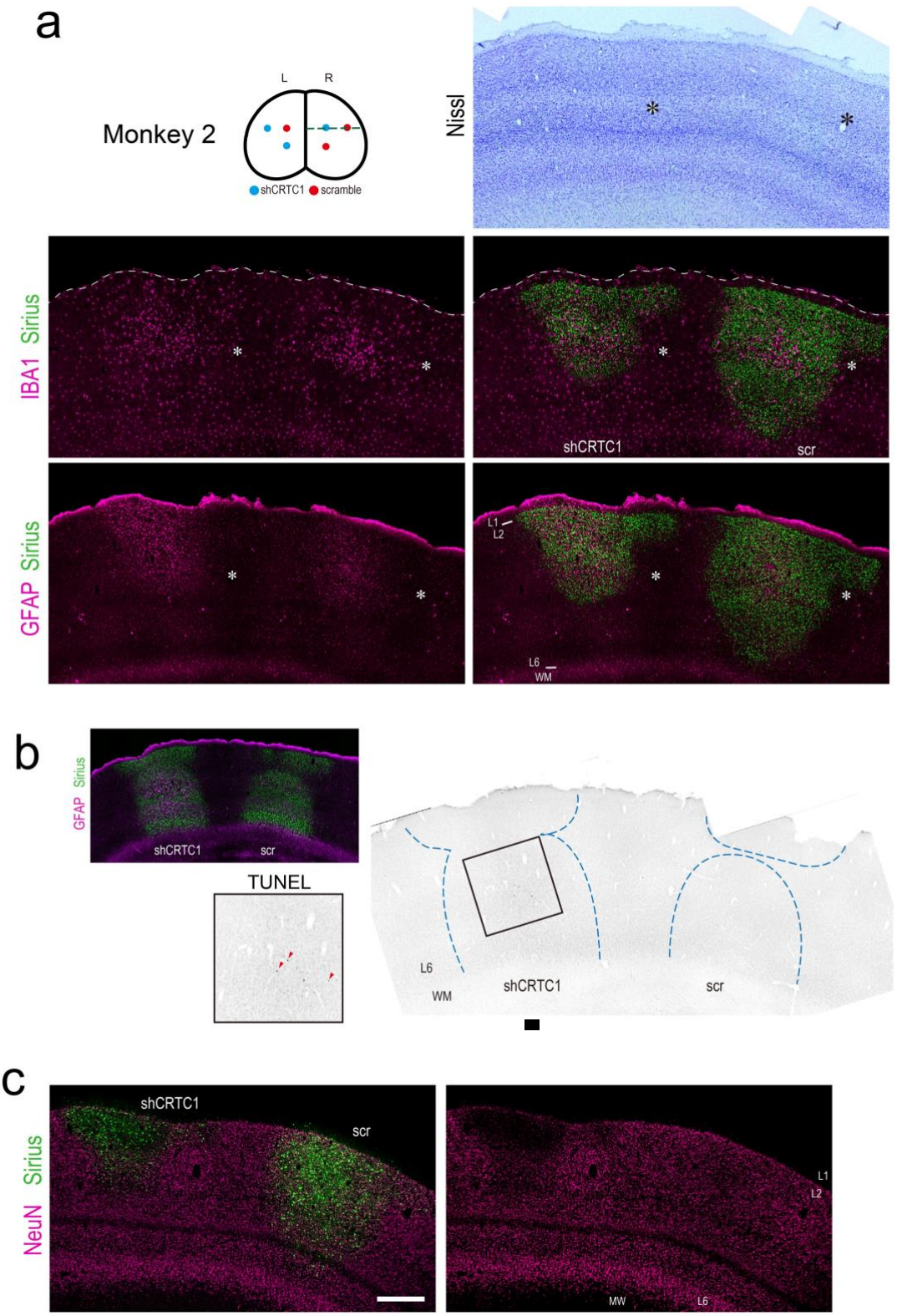

Extended Data Fig. 4. Analysis of glial and cell death markers at the *shCRTC1* and

***shscr* injection sites. a,** TOP left: Analysis of the glial and cell death markers in Monkey 2 at the *shCRTC1*#1 and *shscr* injection sites shown as filled blue circles and red circles, respectively. Top right: Nissl staining. In Monkey 2, we observed only local IEG expression (Fig. 2a, Supplementary Table 2). IBA1 (middle row) and GFAP (bottom row) expressions are shown in magenta. The merged image of either IBA1 or GFAP signals with Sirius signals is shown in the right column. **b,** Top left: the injection sites of *shCRTC1*#1 and *shscr*, left and right, respectively. GFAP (magenta) and Sirius (green). TUNEL signals were detected only at the *shCRTC1*#1 injection site. The square region on the right panel is magnified in the lower left view. **c,** Left: Merged signals with Sirius (green) and NeuN signals. Right: Only NeuN signals are shown. Layers 1, 2, 6 and white matter are abbreviated as L1, L2, L6, and WM, respectively.

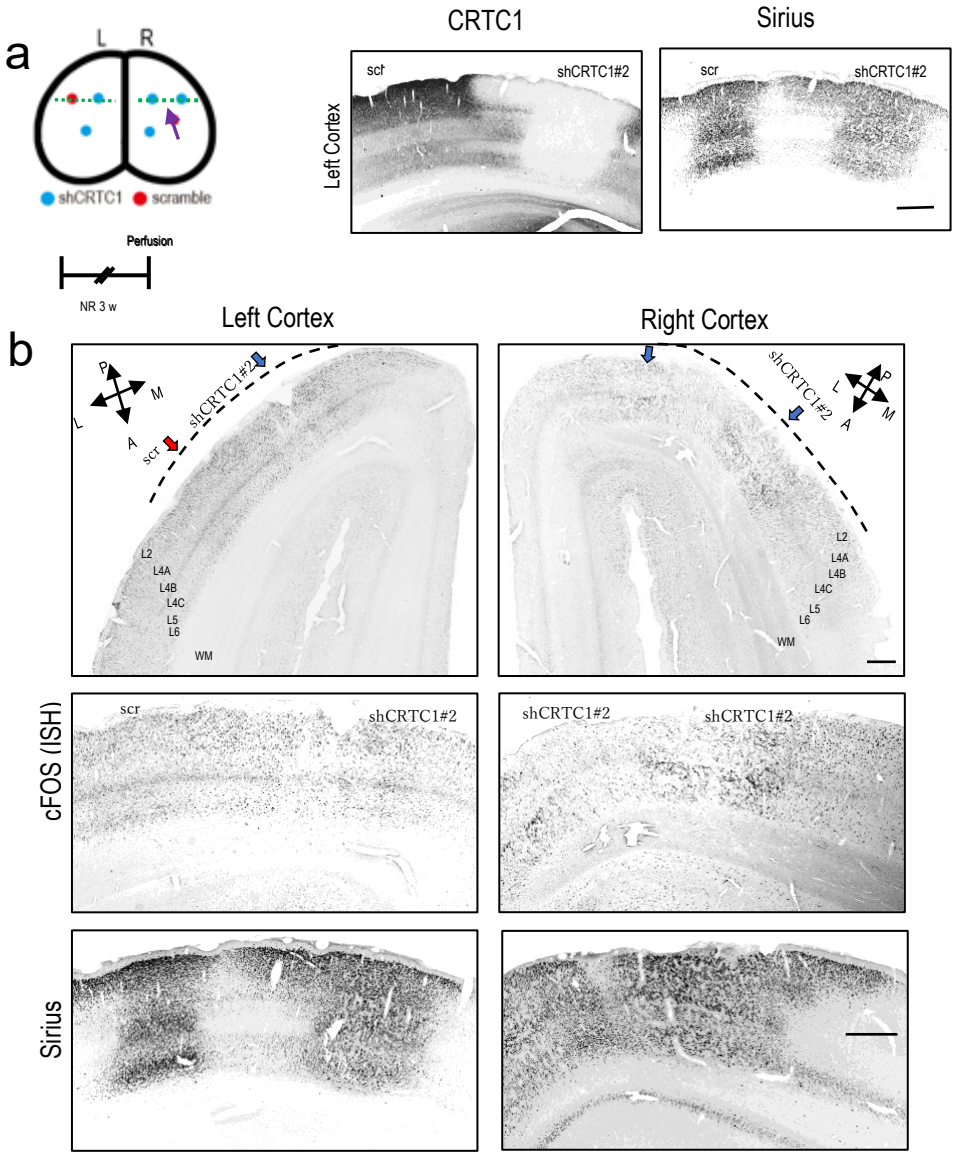

Extended Data Fig. 5. *cFOS* expression at *shCRTC1*#2 injection sites. a, Left: the injection sites in V1 hemispheres (top) and experimental condition (bottom) before sacrifice in Monkey 10 (same as in Extended Data Fig. 6). Middle and right panels: CRTC1 (IHC) and Sirius (IHC) signals at the *shscr* and *shCRTC1*#2 injection sites. **b,** Top row: A low magnification view of *cFOS* expression detected by ISH. L: lateral, M: medial, P: posterior, R: rostral. *shCRTC1*#2 injection sites are indicated by blue arrows,

and the *shscr* injection site is indicated by a red arrow. Note that *cFOS* expression was extended beyond the *shscr* injection site in the left cortex, and that the right V1 injections of *shCRTC1*#2 and *shscr* partially overlap in the cutaway view. Middle and bottom rows; Larger views of the V1 cortex below the dotted regions shown in the top figures are rotated approximately 90° clockwise (left cortex) or counterclockwise (right cortex). Middle and bottom rows show *cFOS* and *Sirius* signals detected by ISH and IHC, respectively, in the adjacent section. Scale bars: 500 μm.

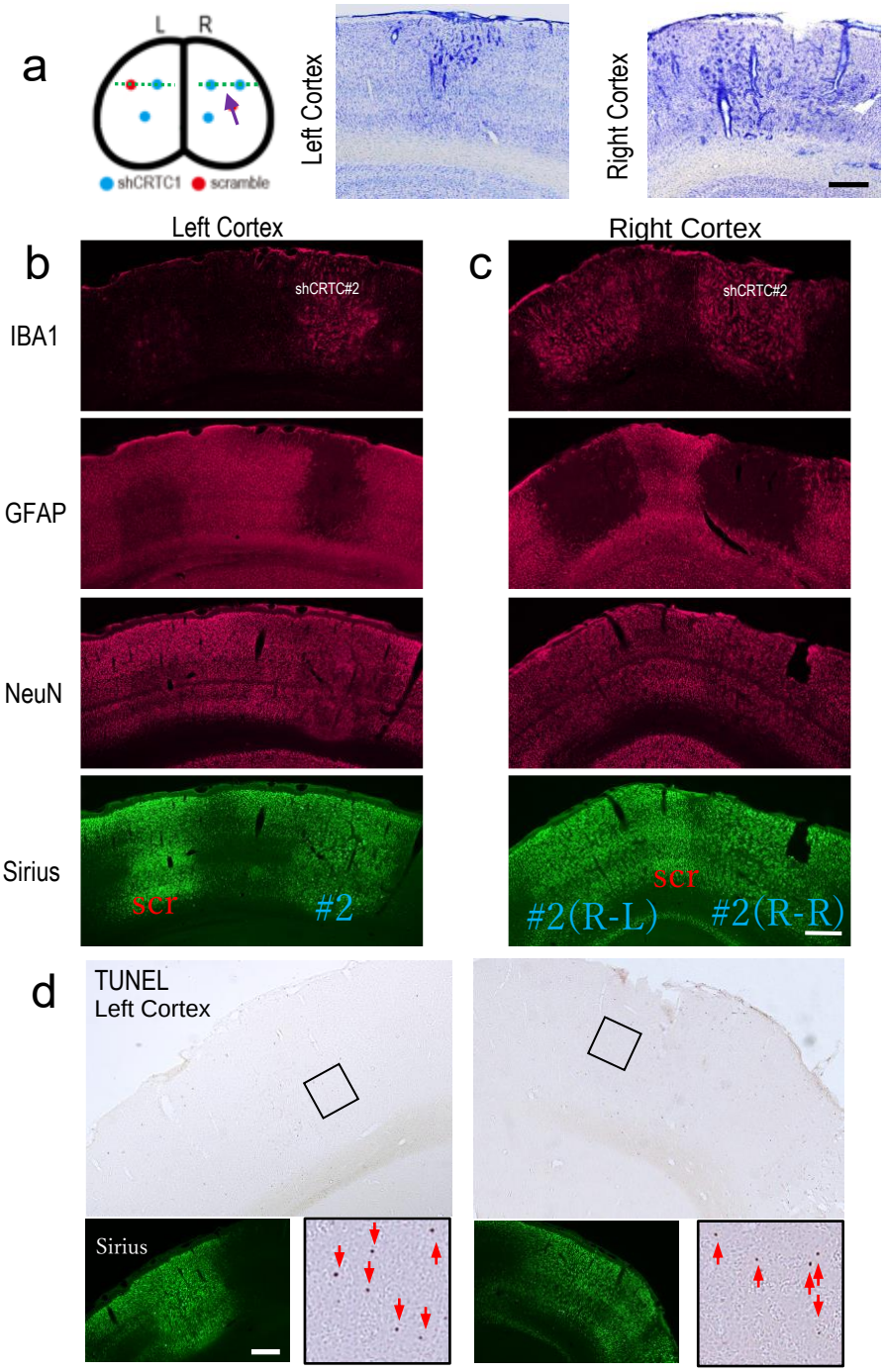

Extended Data Fig. 6. *shCRTC1*#2 injection. a, Left: *shCRTC1*#2 injection sites shown from a posterior view, similar to Fig. 1b. Middle and right: Nissl staining at the *shCRTC1* injection sites in the left and right cortices, respectively. **b,** Injection into the

left V1 cortex. Expression of IBA1, GFAP, NeuN, and Sirius at the injection site from top to bottom. The injection sites of *shscr* and *shCRTC1*#2 are indicated by red and blue letters, respectively, in the Sirius (IHC) staining figure. **c,** Injection into the right V1 cortex. IBA1, GFAP, and NeuN signals are shown in magenta. Sirius signals are shown in green (bottom). Injection sites for *shscr* and *shCRTC1*#2 are shown as in b using red and blue letters. Note that in the view of the bottom figure (Sirius), the injection sites for *shCRTC1*#2 and *shscr* are partially overlap due to the angle of the cross-section, as indicated by the purple arrow in a. **d**, Top row: Low-magnification TUNEL stained images of the left and right V1 cortices. Bottom row: Each image pair shows Sirius and enhanced TUNEL signals (in the region shown in the top image) in the left and right cortices.

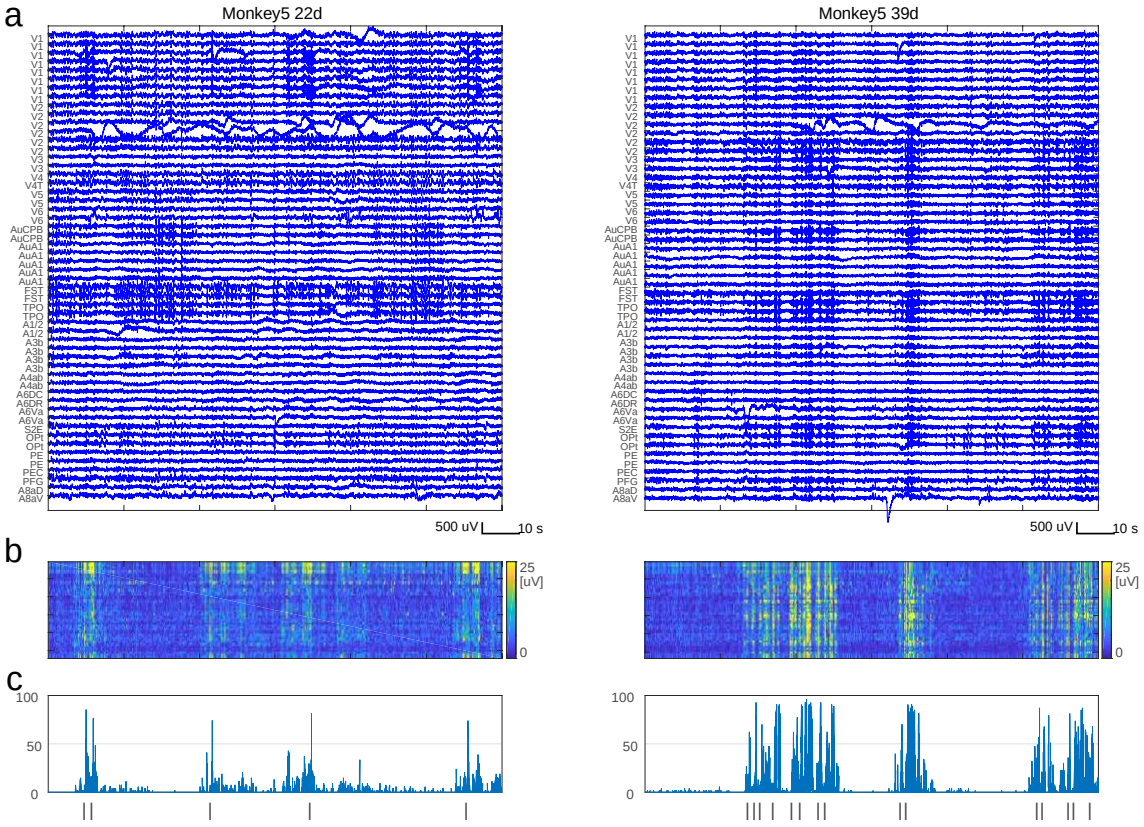

Extended Data Fig. 7. ECoG signals from Monkey 5. a. Examples of raw ECoG signals for 2 minutes. The x-axis is time, and the y-axis is the electrode alignment. The amplitude (μv) is also shown in the time scale (s) in the lower right corner of each panel. **b.** Example of the HFA (80-200 Hz) from Monkey 5. The x-axis is the time in the same range as a, and the y-axis is the electrode arrangement, which are sorted in the same order as a. **c.** Ratio of electrodes showing HFOs (HFA>3 SD) at each time point. Horizontal lines indicate the ratio of 0.5 criterion for cortical-wide HFO (cwHFO). The x-axis is time, in the same range as in a. Vertical bars at the bottom of the figures indicate the times at which the cwHFO occurred.

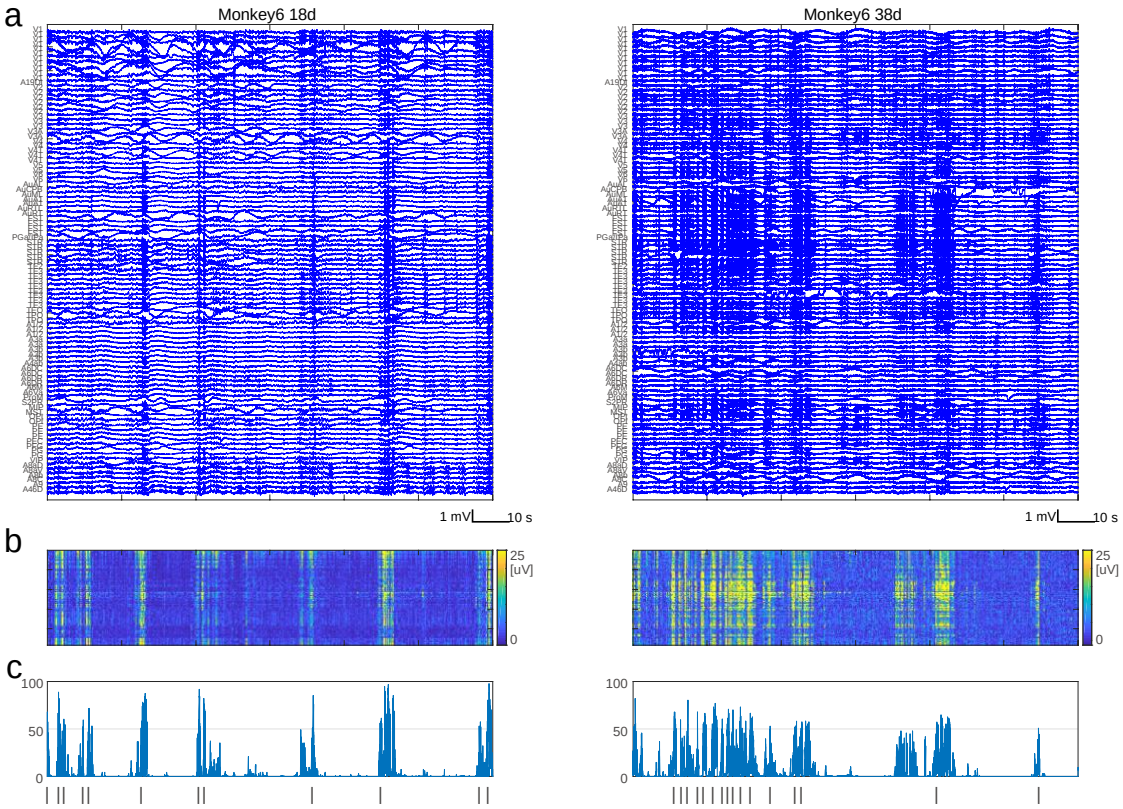

Extended Data Fig. 8. ECoG signals of Monkey 6 on different days after the injection.

ECoG signals of Monkey 6 on days 18 (left) and 38 (right) after the injection, similar to Extended Data Fig. 7. **a,** Examples of raw ECoG signals over a period of 2 min. **b,** Examples of HFA (80-200 Hz) of Monkey 6. **c,** Ratio of electrodes showing HFOs (HFA>3 SD) at each time point. The vertical bars at the bottom indicate the onset of the cwHFOs, as in the previous figure.

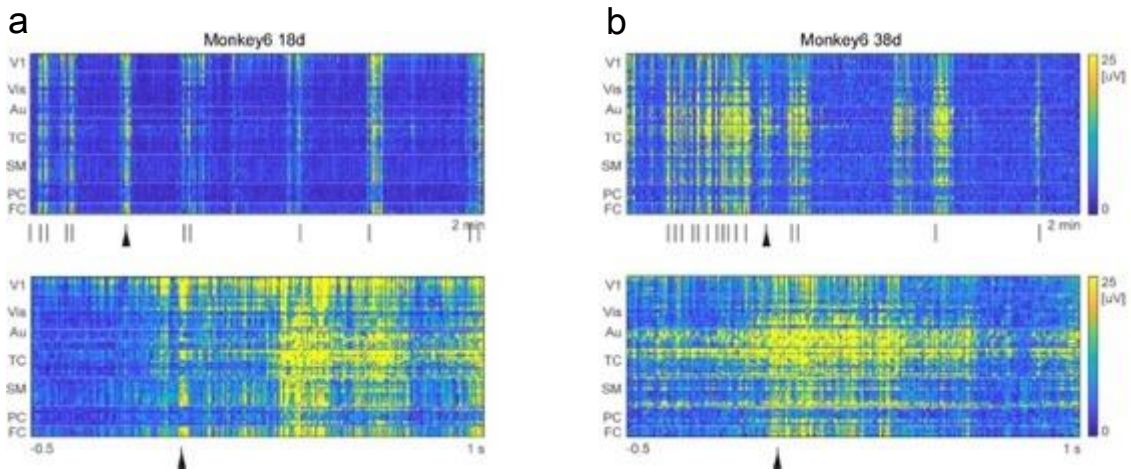

Extended Data Fig. 9. cwHFOs following HFOs in V1 (left) and TC (right) in Monkey 6. The cwHFOs followed the HFOs in the V1 and TC in Monkey 6. **a,** 18 days after injection, **b,** 38 days after injection. Top: Examples of HFA (80-200 Hz). The vertical bars at the bottom of the figures indicate the onset of the cwHFOs. The filled triangles correspond to the onset of the cwHFO magnified in the lower panels. Bottom: Examples of magnified cwHFO following an HFO in V1 (left) and TC (right) in a short time window (from -0.5 to 1 s).

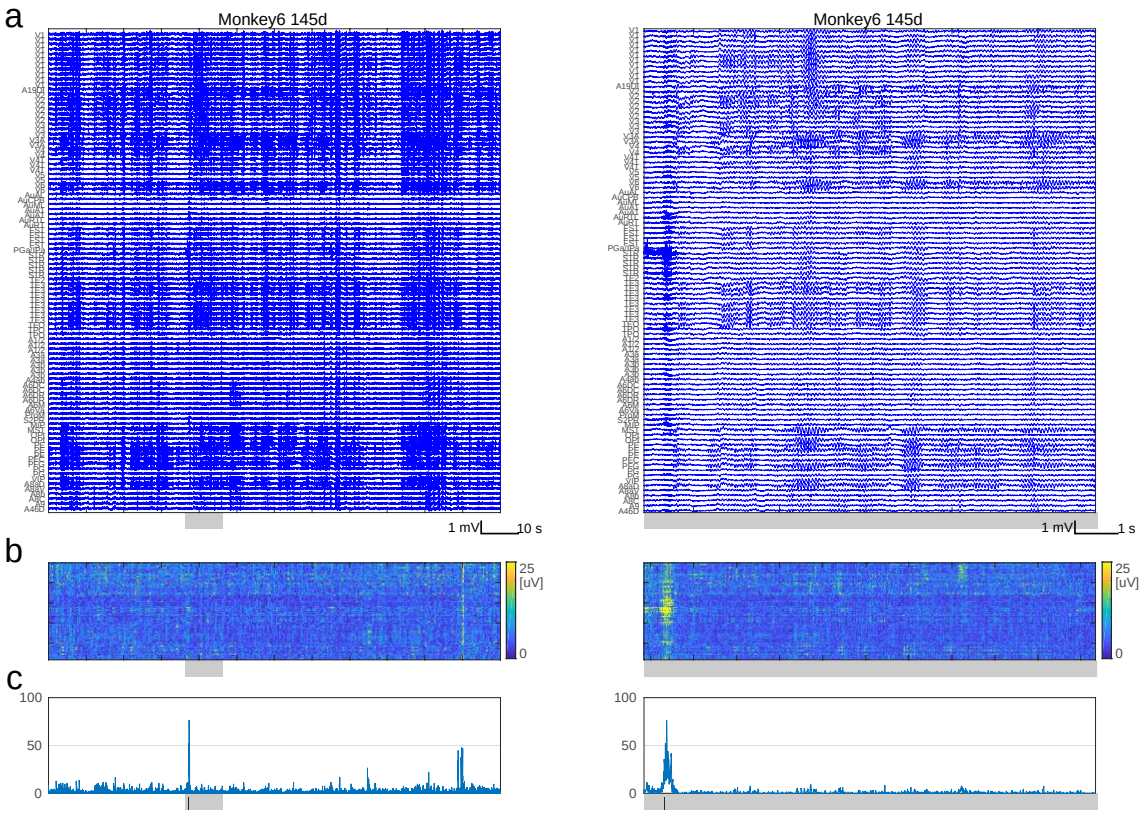

Extended Data Fig. 10. ECoG signals of Monkey 6 late (145 days) after KD. a, Examples of raw ECoG signals over periods of 2 min (left) and 10 s (right). The shaded area on the x-axis of the left figure corresponds to the time range of the right figure. **b,** Examples of HFA (80-200 Hz). The x-axis is time, corresponding to the same range as in a, and the y-axis is the electrodes, which are sorted in the same order as in a. **c,** Ratio of electrodes showing HFOs (HFA>3 SD) at each time point. The thin horizontal line indicates the 0.5 criterion for a cwHFO. The x-axis is time, corresponding to the same range as in a, and the vertical bars at the bottom of the figures indicate the onset of the cwHFOs.